

Fluid-controlled deformation in blueschist-facies conditions: plastic vs brittle behaviour in a brecciated mylonite (Voltri Massif, Western Alps, Italy)

C. MALATESTA*†, L. FEDERICO*, L. CRISPINI* & G. CAPPONI*

*DISTAV, University of Genoa, corso Europa 26, 16132 Genoa, Italy

(Received 17 June 2016; accepted 24 November 2016; first published online 25 January 2017)

Abstract – A blueschist-facies mylonite crops out between two high-pressure tectono-metamorphic oceanic units of the Ligurian Western Alps (NW Italy). This mylonitic metabasite is made up of alternating layers with different grain size and proportions of blueschist-facies minerals.

The mylonitic foliation formed at metamorphic conditions of $T = 220\text{--}310\text{ °C}$ and $P = 6.5\text{--}10$ kbar. The mylonite shows various superposed structures: (i) intrafoliar and similar folds; (ii) chocolate-tablet foliation boudinage; (iii) veins; (iv) breccia.

The occurrence of comparable mineral assemblages along the foliation, in boudin necks, in veins and in breccia cement suggests that the transition from ductile deformation (folds) to brittle deformation (veining and breccia), passing through a brittle–ductile regime (foliation boudinage), occurred gradually, without a substantial change in mineral assemblage and therefore in the overall $P\text{--}T$ metamorphic conditions (blueschist-facies).

A strong fluid–rock interaction was associated with all the deformative events affecting the rock: the mylonite shows an enrichment in incompatible elements (i.e. As and Sb), suggesting an input of fluids, released by adjacent high-pressure metasedimentary rocks, during ductile deformation. The following fracturing was probably enhanced by brittle instabilities arising from strain and pore-fluid pressure partitioning between adjacent domains, without further external fluid input.

Fluids were therefore fixed inside the rock during mylonitization and later released into a dense fracture mesh that allowed them to migrate through the mylonitic horizon close to the plate interface.

We finally propose that the fracture mesh might represent the field evidence of past episodic tremors or ‘slow earthquakes’ triggered by high pore-fluid pressure.

Keywords: mylonite, fluids, ductile–brittle transition, blueschist metamorphism, foliation boudinage, Western Alps, slow earthquakes.

1. Introduction

Fluids are a key component in subduction zones, promoting the transfer of chemical elements from the subducting slab to volcanic arcs, influencing metamorphic reactions and deformation of rocks, and potentially triggering tremors or intra-slab earthquakes (Hacker *et al.* 2003; Bebout, 2007; John *et al.* 2008; Audet *et al.* 2010). The correlations between fluids and veins in subduction zones at high-pressure conditions have been widely studied in eclogite-facies rocks (e.g. Philippot & Selverstone, 1991; Scambelluri *et al.* 1991; Gao & Klemd, 2001; John *et al.* 2008; Spandler, Pettke & Rubatto, 2011; Angiboust *et al.* 2014). These veins formed by locally derived fluids or by episodic infiltration of highly channelized external fluids (Philippot & Selverstone, 1991; Rubatto & Hermann, 2003; John *et al.* 2008; Angiboust *et al.* 2014); the last process probably takes advantage of extensive, interconnected vein networks or lithologic contacts, where mechanical weaknesses between differing lithologies may cause enhanced permeability and facilitate fluid flow

(Breeding *et al.* 2003; Angiboust *et al.* 2014). As a consequence, most high-pressure rocks undergo fracturing either because of their dehydration after increase in metamorphic conditions (i.e. blueschist to eclogite transition) or because of incoming fluids released by other lithologies (e.g. John *et al.* 2008). Philippot & Selverstone (1991), observing a foliated eclogitic metagabbro in the Monviso ophiolitic complex (Western Alps), concluded that a continuous fluid-assisted interaction between ductile and brittle deformation affected the metagabbro body and pulses of fluids were associated in time with increments of shear and tensile failure.

Large-scale fluid pathways have been observed both along the subduction interface and inside the slab itself (Bebout & Barton, 1989; Breeding, Ague & Bröcker, 2004; Angiboust & Agard, 2010; Angiboust *et al.* 2014; Scambelluri *et al.* 2014, 2016; Bebout & Penniston-Dorland, 2016). Experimental studies indicate that some fluids are released from the subducting slab through discontinuous or continuous reactions at almost any depths in the range 70–300 km (Peacock, 1993; Schmidt & Poli, 1998; Ulmer & Trommsdorff, 1999); the major pulse of fluid release from

† Author for correspondence: cristina.malatesta@unige.it

the oceanic crust occurs at *c.* 50–70 km depth (Peacock, 1993; Schmidt & Poli, 1998), whereas at shallow depths (<15 km) most of the fluids are expelled through porosity collapse and diagenesis, and collected via large fault systems (Le Pichon, Henry & Lallemand, 1990; Moore & Vrolijk, 1992). Thermodynamic studies indicate that along an average geotherm ($6\text{ }^{\circ}\text{C km}^{-1}$) characterizing present-day subduction zones, H_2O release from subducted sediments is concentrated in a depth range of *c.* 70–100 km and metabasalts mostly dehydrate at depths of 80–120 km (Li *et al.* 2008).

Despite these numerous studies, some open questions still remain about the mechanisms of release, infiltration and migration of fluids through the slab–mantle interface and inside the slab (Breeding *et al.* 2003; John *et al.* 2008; Angiboust *et al.* 2014): how are fluids extracted and concentrated in the rocks, leading to infiltration towards the overriding plate, mobilizing chemical elements? what is the origin of fluids migrating along the slab and what is the length scale of the fluid flow? in what way is fluid circulation correlated with deformation under high-pressure conditions?

In this paper, we present the study of a blueschist mylonitic body that occurs at the contact between two metamorphic ophiolitic units: the blueschist Montenotte Unit and the eclogitic Voltri Unit (Ligurian Western Alps; Federico *et al.* 2014). The blueschist mylonitic metabasite (hereafter MM) was affected by complex deformations, evolving from ductile (*i.e.* folding) to brittle–pervasive veining and brecciation at relatively constant *P–T* conditions. The body was permeated by fluids expelled by metasediments during ductile deformation, whereas fracturing was triggered by internal fluids.

The aim of this paper is:

- (i) to describe the structural and petrographic features of the MM, with *P–T* determinations of climax metamorphism via *P–T* pseudosection computation;
- (ii) to discuss the progressive deformation of the MM and the role of fluids influencing the plastic vs brittle behaviour of rocks, including the possible relations with seismicity;
- (iii) to discuss such structural and metamorphic evolution in the framework of the alpine subduction and the provenance of fluids.

2. Geological setting

The study area is located at the limit between two tectono-metamorphic units: the Montenotte and Voltri units (Capponi *et al.* 2013, 2015; Federico *et al.* 2014). The two units pertain to the internal Ligurian–Piedmontese domain of the Western Alps (Fig. 1) (Vanossi *et al.* 1984); they represent a fragment of the Mesozoic Ligurian–Piedmontese ocean subducted during Cretaceous to Eocene time below the Apulian margin; the continental collision between Europe and

Adria during the Middle Eocene led to the building of the Western Alpine chain and to the present architecture of the study area (*e.g.* Vanossi *et al.* 1984; Polino, Dal Piaz & Gosso, 1990; Ford, Duchêne & Gasquet, 2006).

Both the Montenotte and Voltri units pertain to the Voltri Massif which has been interpreted as a fossil plate-interface domain now exposed to the surface (Federico *et al.* 2007; Malatesta *et al.* 2012b; Scambelluri & Tonarini, 2012; Scambelluri *et al.* 2016).

2.a. The Montenotte Unit

The Montenotte Unit crops out in the central-western part of Liguria, W-SW of the Voltri Unit (Figs 1, 2); it encompasses a metamorphosed ophiolitic succession, made up of predominant metagabbro (both Fe- and Ti-oxide-rich and Mg-rich varieties), metabasalt and serpentinite, plus the metamorphosed sedimentary cover comprising metachert, meta-limestone and phylladic schist. The metamorphic stage in blueschist-facies conditions (Table 1a) produces an assemblage of albite + chlorite + Na-amphibole \pm Na-pyroxene \pm lawsonite \pm pumpellyite \pm epidote in metagabbro (Cabella *et al.* 1994; Cortesogno *et al.* 2002; Capponi *et al.* 2013), pointing to conditions of *c.* 1.1 GPa and $340 \pm 20\text{ }^{\circ}\text{C}$ (Desmons, Compagnoni & Cortesogno, 1999 and references therein). Late greenschist-facies overprint occurs in places and is mainly detectable in the Fe- and Ti-oxide-rich metagabbros, with actinolite and albite blastesis (Federico *et al.* 2014).

From the structural point of view, the Montenotte Unit is characterized by two folding phases coeval with the blueschist-facies metamorphism (D_1 and D_2 , Table 1a; Beccaluva *et al.* 1979; Anfossi, Colella & Messiga, 1984; Capponi *et al.* 2013). The $D_1 + D_2$ folding gives rise to Type 3 interference patterns (Ramsay & Huber, 1987), traceable up to the map scale in the study area (Fig. 2; Federico *et al.* 2014). The most evident foliation in the field is commonly a composite fabric that contains the D_1 - and D_2 -related schistosity, and which in this area is mainly NW–SE striking; such composite fabric controls the contacts among lithologies.

A later phase of open to gentle, sub-cylindrical folding, with rare axial plane cleavages (D_3 ; Beccaluva *et al.* 1979; Anfossi, Colella & Messiga, 1984; Capponi *et al.* 2013), is coeval with low greenschist-facies metamorphic conditions (Capponi *et al.* 2013) and is shared with the Voltri Unit (Federico *et al.* 2014).

Contractional structures of Aquitanian – early Burdigalian age are represented by long-wavelength open folds and thrusts (D_4 of Capponi & Crispini, 2002), with top-to-the-E-NE vergence. This phase is shared with the Voltri Unit (Federico *et al.* 2014).

2.b. The Voltri Unit

The Voltri Unit (Capponi & Crispini, 2008; Capponi *et al.* 2015) crops out at the southeastern termination

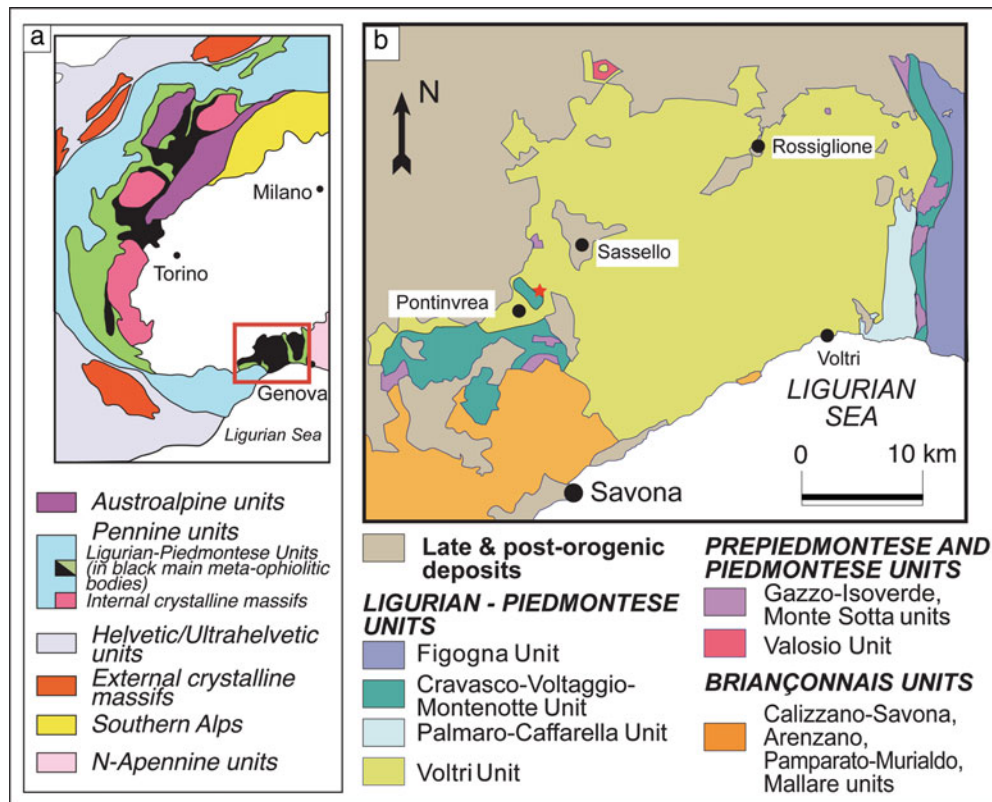


Figure 1. (Colour online) (a) Sketch of the NW Alps (box locates area of (b)); (b) Simplified geological map of the easternmost Ligurian Alps (red star locates the studied outcrop).

Table 1. Synoptic table summarizing the metamorphic and deformative events in (a) the Montenotte and (b) Voltri units (modified after Federico *et al.* 2014), and in (c) the studied mylonite outcrop in between (this work).

a. Montenotte Unit			
Deformation phase*	Metamorphic conditions	Assemblage(in mafic rocks)	Fabric
D _{1mt}	blueschist	ab + chl + Na-amph ± Na-py ± lws ± pump ± ep	CF _{mt}
D _{2mt}	low greenschist	act/ab blastesis	axial plane cleavage
D ₃	non-metamorphic	/	none
D ₄			
b. Voltri Unit			
Deformation phase	Metamorphic conditions	Assemblage (in mafic rocks)	Fabric
D _{1vt}	(Na-amphibole greenschist)–greenschist	act + ep + chl + ab ± spn	CF _{vt}
D _{2vt}	low greenschist	act/ab blastesis	axial plane cleavage
D ₃	non-metamorphic	/	none
D ₄			
c. Mylonite			
Deformation phase	Metamorphic conditions	Assemblage	Fabric
D _{1my}	blueschist	Na-amph + ep + wm ± spn ± Fe-ox ± qtz ± ap	CF _{my}
D _{2my}			/
EPF _{my}	blueschist	Na-amph + ep + wm + qtz ± Fe-ox ± spn ± ap	mylonitic foliation foliation boudinage, veining, breccia
D ₃	low greenschist	act/ab blastesis	axial plane cleavage

*Subscripts ‘mt’, ‘vt’ and ‘my’ refer to ‘Montenotte’, ‘Voltri’ and ‘mylonite’ respectively. In the mylonite outcrop the concentration of deformation triggered the development of a peculiar structural evolution, possibly independent of the adjoining rocks; as a result, D_{1my} and D_{2my} folds have no direct correlation with D_{1mt} and D_{2mt} folds of the Montenotte Unit, albeit developed under the same blueschist facies metamorphic conditions (Federico *et al.* 2014).

of the Western Alps, E-NE of the Montenotte Unit (Fig. 1b). It includes metamorphic ophiolitic rocks with metasediments and slices of subcontinental lithospheric mantle (Chiesa *et al.* 1975; Piccardo, 1977; Rampone *et al.* 2005). Meta-ophiolites are serpent-

inite, metagabbro and metabasite, and are associated with calcschist, minor mica- and quartz-schist; mantle rocks encompass lherzolite and harzburgite with minor pyroxenite and dunite. The Voltri Unit re-equilibrated at peak eclogite-facies conditions, with the growth

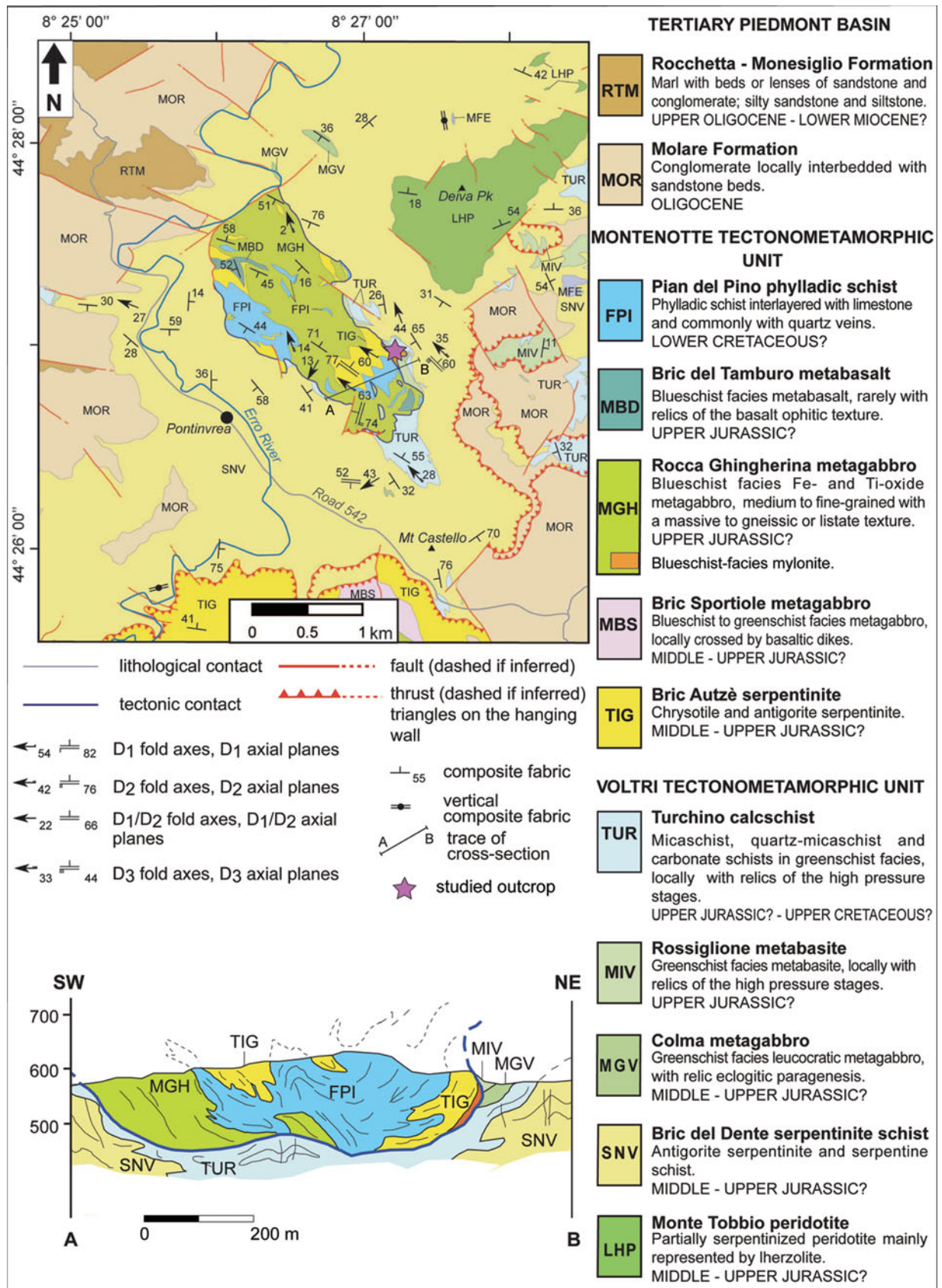


Figure 2. (Colour online) Geological map and cross-section of the study area (star locates the studied outcrop). The Montenotte and Voltri units and the mylonite at the contact are all deformed by a regional-scale D₃ fold with NW–SE-trending, NW-plunging axis.

of garnet + omphacite + rutile + Na-amphibole ± phengite ± clinozoisite in Fe-rich metagabbro (e.g. Ernst, 1976; Bocchio, 1995), corresponding to metamorphic conditions of $P=18\text{--}22$ kbar and $T=500\text{--}600$ °C (e.g. Messiga, Piccardo & Ernst, 1983; Liou *et al.* 1998; Brouwer, Vissers & Lamb, 2002; Federico *et al.* 2004) achieved at *c.* 50 Ma (Federico *et al.* 2005). A later partial re-equilibration in greenschist-facies conditions affected the Voltri Unit during the Early Oligocene (Federico *et al.* 2005) and is particularly pervasive in metasedimentary rocks.

Several deformational events have been described in this unit (Table 1b; Vanossi *et al.* 1984; Capponi & Crispini, 2002, 2008; Malatesta *et al.* 2012a): the oldest structures are eclogite-facies foliation and rootless hinges of isoclinal folds, which have no continuity across outcrops. The most pervasive structures are tight to isoclinal transpositive D_1 and D_2 folds, developed in metamorphic conditions ranging from Na-amphibole greenschist facies to greenschist facies *sensu stricto* (Crispini & Frezzotti, 1998; Capponi & Crispini, 2002). Their superposition gives rise to a Type 3 interference pattern (Ramsay & Huber, 1987), and the superposition of D_1 and D_2 schistosity produces a Composite Fabric that controls contacts among different lithologies.

The later D_3 event is shared with the Montenotte Unit and is coeval with low greenschist-facies metamorphic conditions. F_3 folds are usually parallel folds, gentle to open in shape, in places associated with a roughly spaced cleavage.

The D_4 event is also shared with the Montenotte Unit (Federico *et al.* 2014) and is expressed by long-wavelength open folds and thrusts, with top-to-the-E-NE vergence.

3. Structural and petrographic data of the mylonite outcrop

The studied MM crops out (Fig. 3) between the Montenotte Unit serpentinite (to the west) and the metasediment/metabasite of the Voltri Unit (to the east); here metasediment and metabasite are interbedded, with cm-thick talcschist layers in between.

The MM is characterized by alternating fine-grained and minor ultra-fine-grained domains (*c.* 10 cm thick). The variations in grain size can potentially be either an inherited original feature later enhanced by deformation (i.e. presence of basaltic dykes and/or pillows) or a result of the mylonitization processes.

As described in the following paragraphs, we observed several superposed structures formed at the same metamorphic conditions: this indicates that the MM underwent a progressive polyphase deformation history (Figs 4, 5a; Table 1c).

3.a. Ductile and brittle/ductile structures

3.a.1. Folds and schistosity

The oldest deformative event is represented by mm-size intrafoliar folds (D_1 folds; Fig. 6a) and rootless

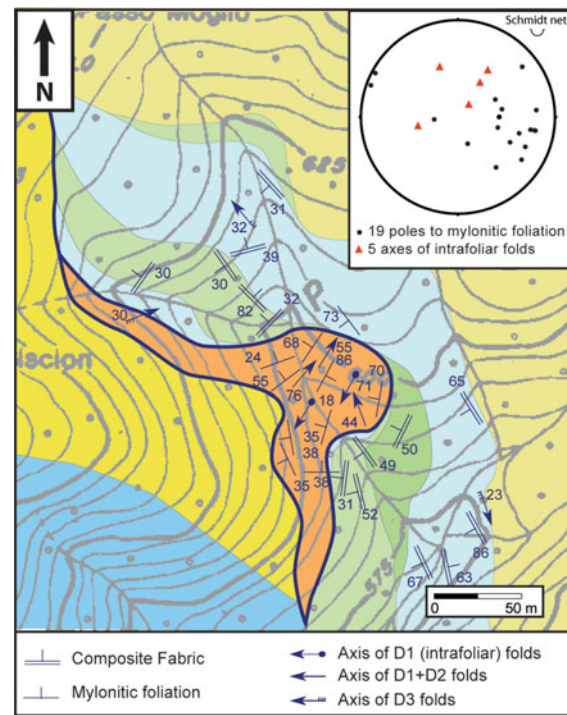


Figure 3. (Colour online) Detailed geological map of the study area (for colour legend see Fig. 2); the equal-area stereonet shows the attitude of main structural features in the MM.

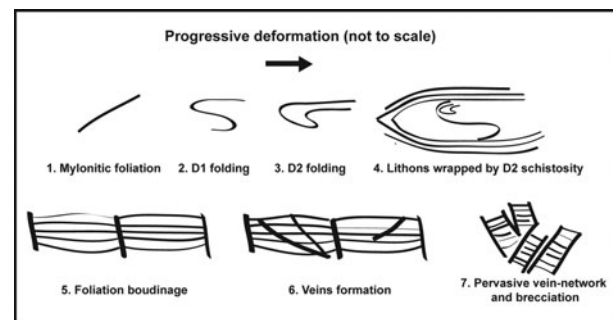


Figure 4. Sketch showing the structures formed by the progressive deformation of the MM.

hinges of folds that deform a fine-grained blueschist mylonitic foliation; D_1 folds are associated with a Na-amphibole-bearing axial plane schistosity. These folds and the related schistosity are deformed by moderately non-cylindrical tight similar folds (D_2 folds) of mm to cm size (Fig. 5a, b); the axes of such folds have a pitch of $60\text{--}80^\circ$ on the axial plane (similar to the ‘reclined folds’ of Ghosh & Sengupta, 1987).

The schistosity associated with the D_2 event is pervasive and the related transposition is severe: lithons in which D_1 and D_2 folds are visible (Fig. 5b) are preserved only locally. In such domains, the superposition of D_1 and D_2 folds gives rise to Type 3 interference patterns (Ramsay & Huber, 1987). In most cases the superposition of D_1 - and D_2 -related schistosity and the former mylonitic foliation results in a Composite Fabric (CF, corresponding to the mylonitic foliation) that

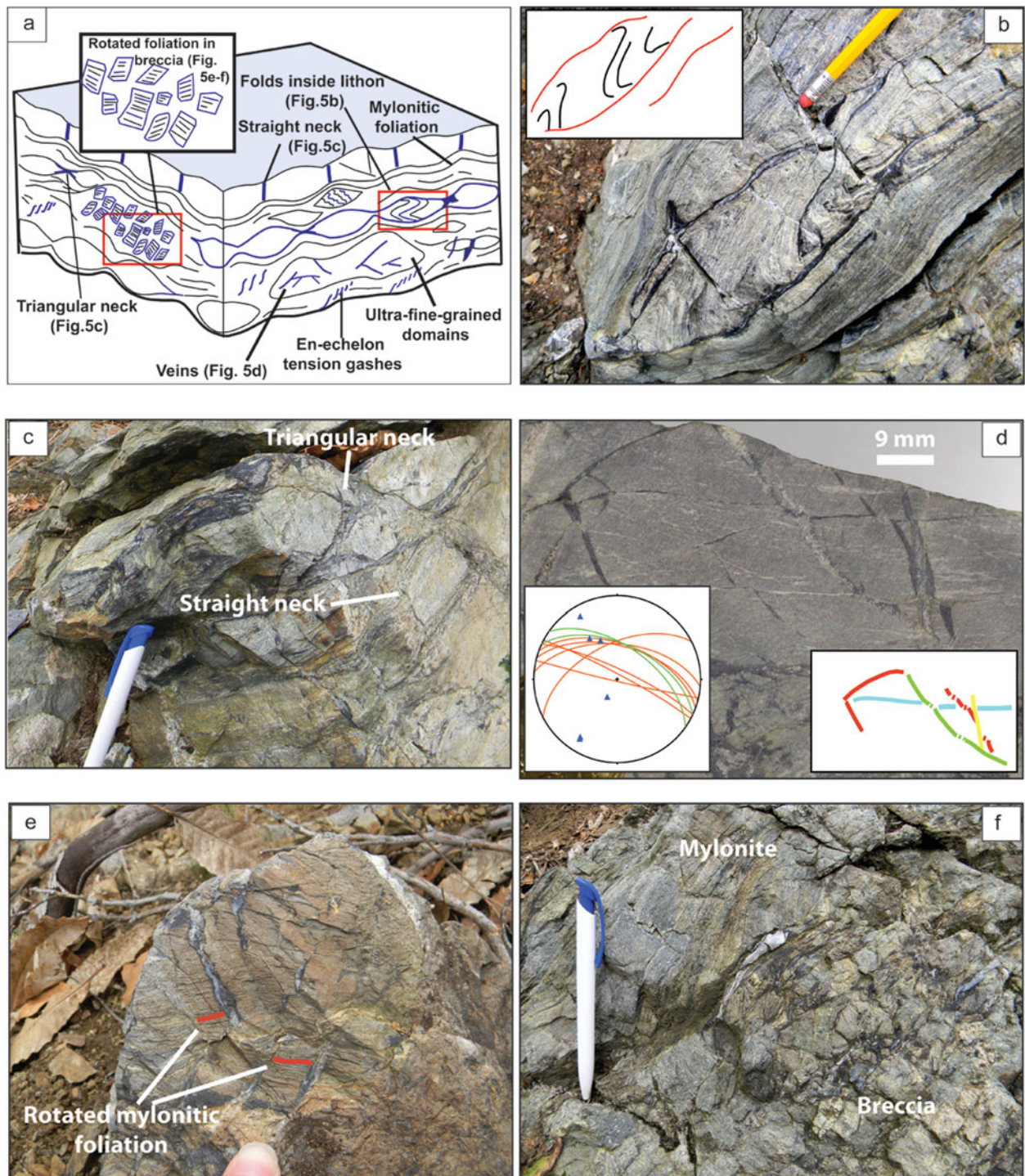


Figure 5. (Colour online) (a) A 3D sketch showing the geometrical relationships between structural elements (see text for description); (b) isoclinal folds preserved in lithons (note the blue-amphibole-rich surfaces); (c) boudins with different neck geometries; (d) several generations of veins cross-cutting the hand specimen; the attitudes of vein set 1 (red line) and 2 (green line) are shown in the equal-area stereonet together with boudin axes (triangles); in the sketch, light-blue line is a Na-amphibole-rich surface, red lines are vein set 1, yellow line is vein set 2 and green line is vein set 3; (e) breccia with veins cutting at high angle the foliation; red lines show the trace of the rotated mylonitic foliation inside different clasts; (f) brecciated domain in contact with unbrecciated MM.

is the most evident structure in the field (Fig. 3). Along the CF we observed asymmetric porphyroclasts, either bluish or whitish, with either a σ or δ geometry.

In fine-grained domains (M1M2, M1M4 samples) both the main foliation (composite fabric) and the folded foliation, preserved inside lithons, show alternating sub-mm-thick layers respectively rich in (i) Na-

amphibole, (ii) epidote, (iii) white mica + epidote and (iv) Fe-oxide (Figs 6b, 7a):

(i) Na-amphibole-rich layers are made by Na-amphibole + minor white mica, Fe-oxides and quartz growing syn-kinematically; Na-amphibole, classified as glaucophane or Mg-riebeckite according to Leake *et al.* (1997) (Fig. 8a), locally replaces as aggregates

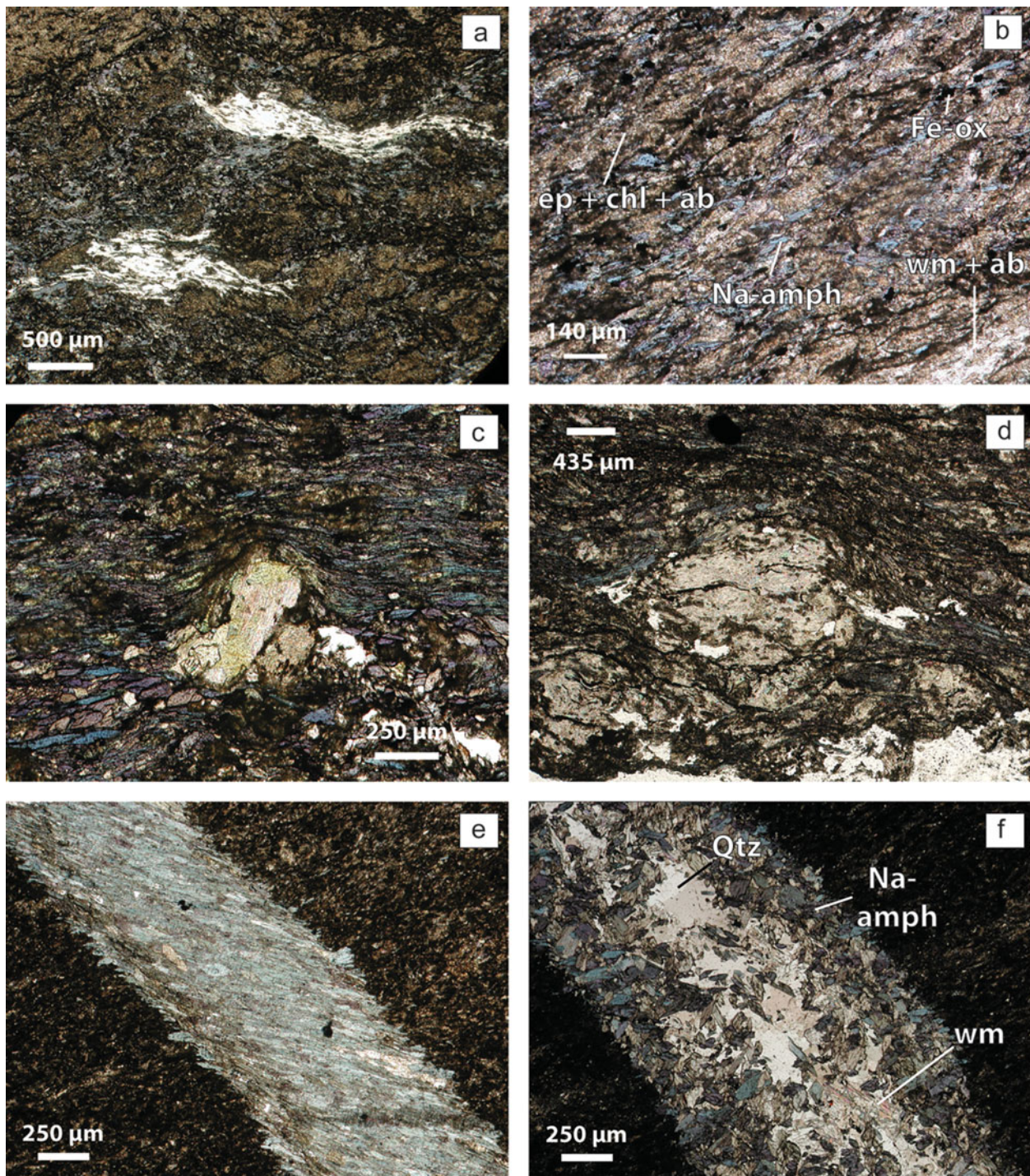


Figure 6. (Colour online) Thin-section photomicrograph. (a) Stretched hinges of intrafoliar folds (fine-grained white mica). Folds developed a pervasive axial plane schistosity and Na-amphibole grew; (b) mylonitic foliation; (c, d) phengite/paragonite + clinozoisite + chlorite pseudomorphs after lawsonite; (e) syntaxial shear vein including Na-amphibole fibres; (f) composite vein.

porphyroclasts occurring along the main foliation. White mica has a phengitic composition and shows large variations of Si content (from 6.11 to 6.86 Si per formula unit (pfu)) (Fig. 8b), with Si content decreasing from cores to rims. The highest Si content is in phengite along the former folded foliation preserved in lithons (M1M4 sample).

(ii) Epidote-rich layers are often cloudy and include fine-grained syn-kinematic epidote + white mica + minor Na-amphibole + sphene + apatite

+ tiny spinels. The chemical composition of epidote varies between the clinozoisite and the Fe-rich epidote end-members; clinozoisite is gradually overgrown by Fe-rich epidote, with Fe content increasing from the core to the rim of the crystal. Quartz grows between Na-amphiboles replacing epidote. Locally aggregates of Na-amphibole + epidote or white mica + minor epidote pseudomorphose former porphyroclasts (σ - and δ -type porphyroclasts), respectively sigmoidal- and rounded/prismatic-shaped

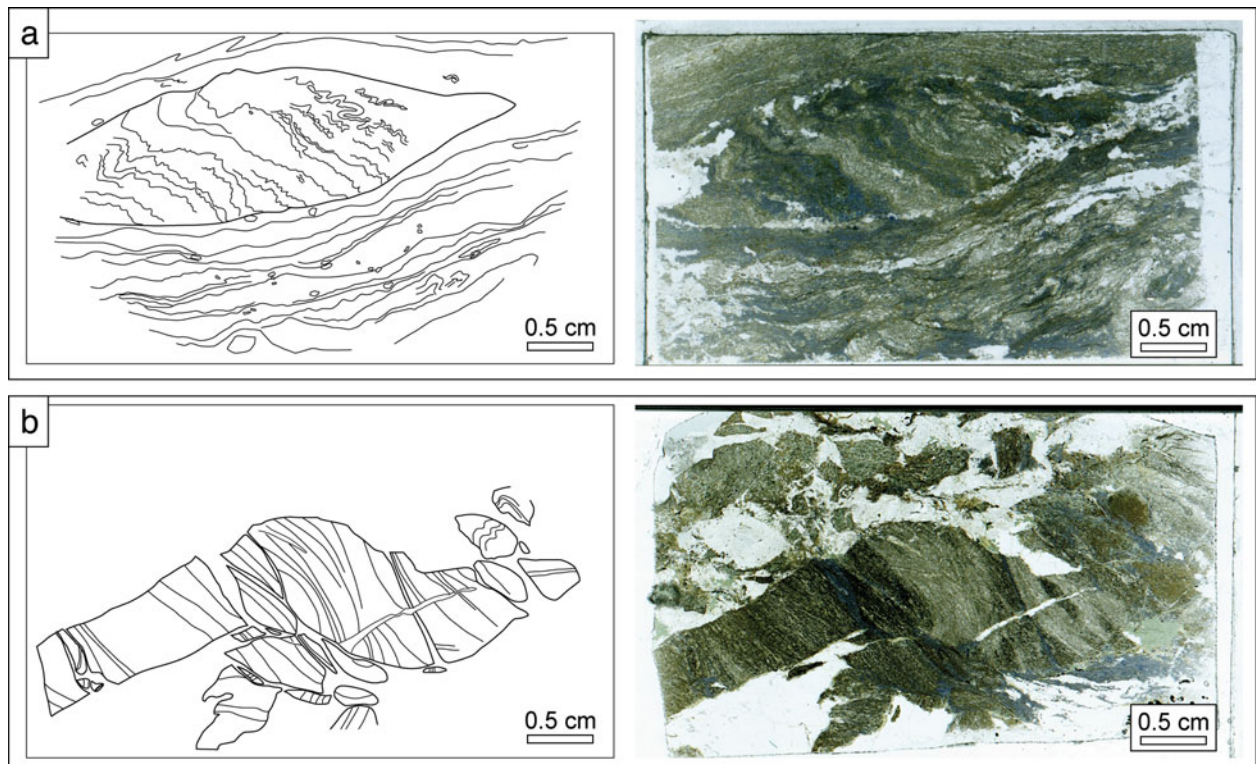


Figure 7. (Colour online) Scan of thin section (right) and its redrawing (left): (a) sample M1M4 shows the folded foliation inside a microlithon wrapped by the main mylonitic foliation; rounded pseudomorphoses on former lawsonite, now made up of fine-grained white-mica \pm minor epidote occur along the main foliation; (b) sample M1M9 shows different breccia clasts with an internal mylonitic foliation (more recent albite-rich veining in the upper left part of the thin section has been omitted for simplicity).

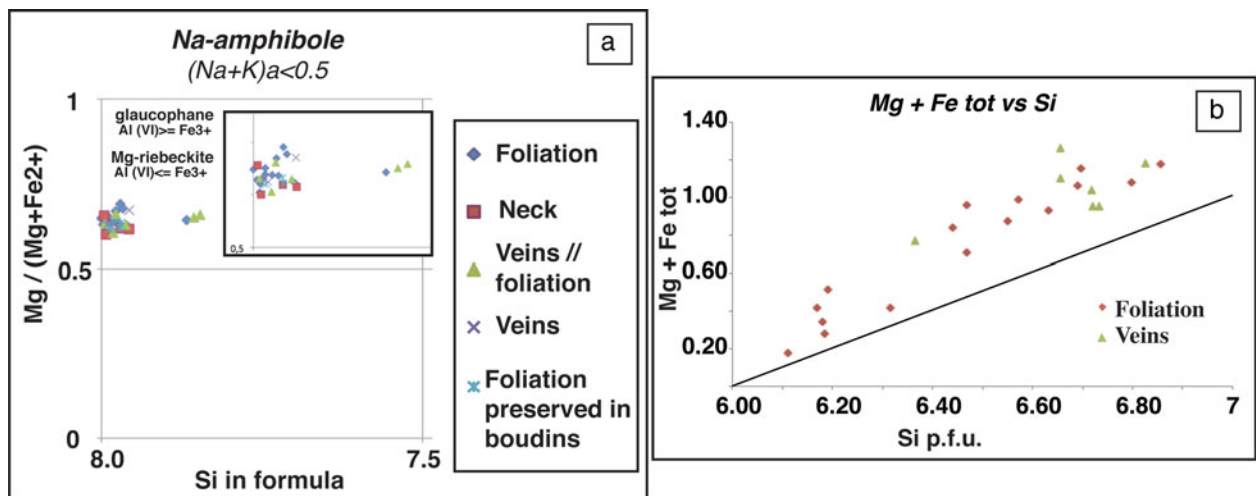


Figure 8. (Colour online) Na-amphibole and white mica composition. (a) Classification diagram of Na-amphibole after Leake *et al.* (1997); (b) white mica ($Mg + Fe_{tot}$) vs Si diagram.

(Fig. 6c, d); porphyroclasts show syn-kinematic Na-amphibole antitaxial strain fringes (Fig. 6d). White mica-rich porphyroclasts often occur along the boundary of mm-size lithons (Fig. 7a), and locally preserve Fe-oxide layers concordant with oxide layers along the main foliation (Fig. 6c, d). White mica includes tiny crystals of epidote and zircon; in pseudomorphoses it is classified as phengite/paragonite; here phengite has the lowest Si value (6.11–6.19 Si pfu).

(ii) Fine-grained syn-kinematic white mica + epidote + rare sphene, Na-amphibole and Fe-oxides occur in white mica-rich whitish layers. Here sphene includes micron-size rutile crystals.

(iv) Fe-oxide-rich layers wrap white mica porphyroclasts occurring along the main foliation. Rare tiny sulphides occur.

Ultra-fine-grained domains (M1M3 and M1M9 samples) have a cloudy texture with a pervasive foliation outlined by layers of (i) Na-amphibole + minor

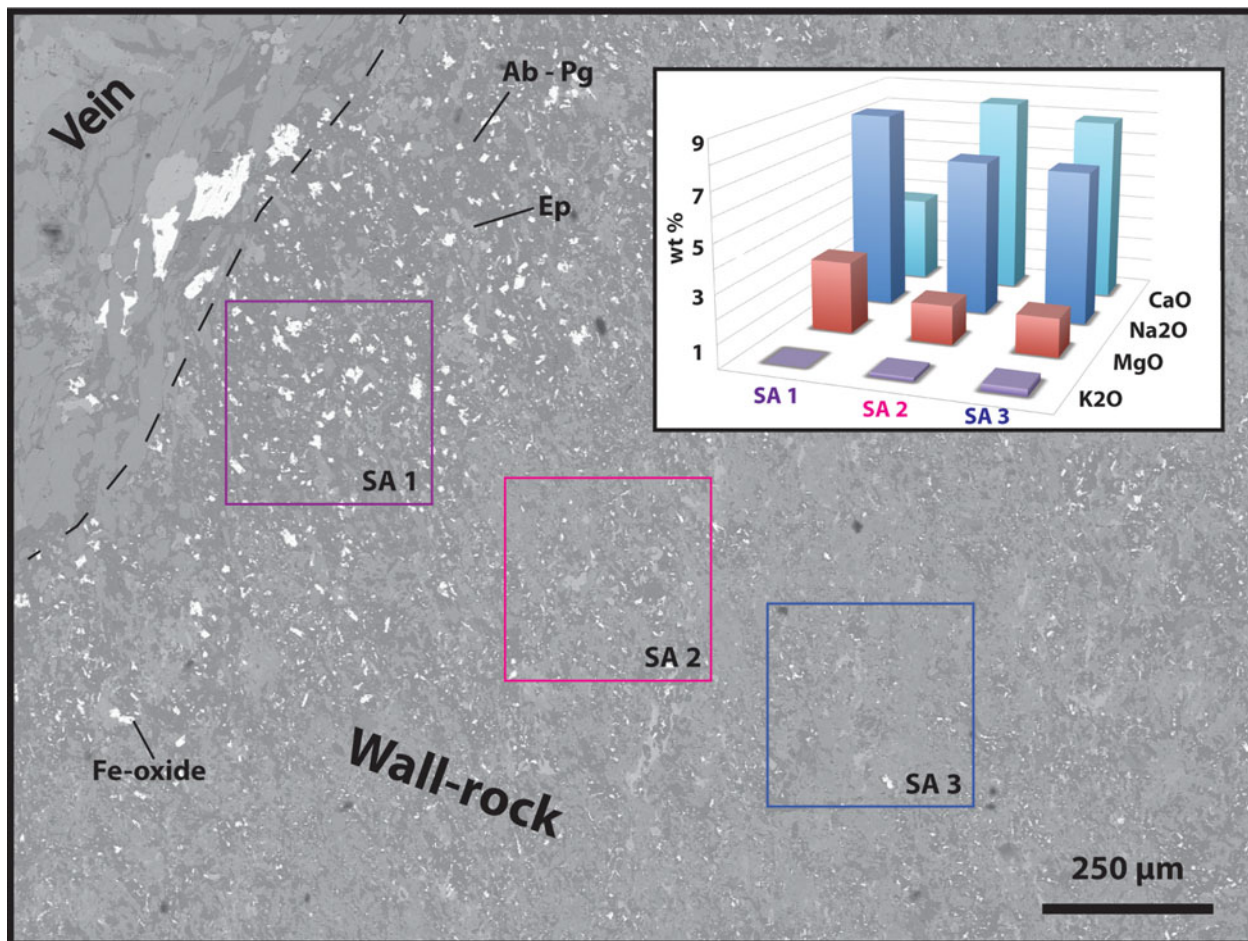


Figure 9. (Colour online) Electron microprobe image and chemical variation of selected areas in the wall rock at different distances from the vein. The mineral abbreviations are after Kretz (1983).

white mica, sphene and apatite; (ii) epidote + white mica + sphene + Ti-V-bearing Fe-oxide-hydroxide + minor Na-amphibole and apatite – rare tiny sulphides occur; and (iii) syn-kinematic fine-grained epidote + fluoro-apatite + minor white mica (whitish layers). Here white mica has been classified as phengite and paragonite; paragonite is syn- to post-epidote, and is overgrown by albite.

Both in fine- and ultra-fine-grained domains, minor chlorite grows between oxides and epidote replacing them. Finally fine-grained albite grows, replacing chlorite, epidote, white mica and locally Na-amphibole. Fe-oxides (haematite), growing together with albite, replace Na-amphibole. Locally, white mica and quartz grow on epidote.

Along the foliation of these two domains, aggregates of either fine-grained (1) Na-amphibole or (2) Na-amphibole + epidote occur, developing Na-amphibole fringes. We interpret aggregates (1) and (2) as pseudomorphoses after pre- to syn-kinematic pyroxene.

The pseudomorphoses made of phengite/paragonite + epidote or uniquely of phengite aggregates could be interpreted as lawsonite (see Faryad & Hoinkes 1999; Able & Brady, 2001), thus indicating that at least the mylonitic foliation formed in lawsonite–blueschist

facies metamorphic conditions; when P – T conditions changed, lawsonite broke down.

3.a.2. Foliation boudinage

A later foliation boudinage (Fig. 5c) affects the composite fabric, and generates boudins visible from the mm to the outcrop scale, wrapped by Na-amphibole-rich surfaces (syn-kinematic Na-amphibole fibres + minor epidote and fine-grained sphene or Na-amphibole + minor white mica + apatite + rare Fe-oxides + tiny sphene replacing rutile), which mark the transition to the main mylonitic foliation.

Boudinage has a dominantly symmetric chocolate-tablet structure (Fig. 5a) with a minor asymmetric component, suggested by Na-amphibole-bearing en échelon tension gashes. Boudin necks, often joining up with Na-amphibole-rich surfaces wrapping them, are filled by syn-kinematic Na-amphibole or Na-amphibole + quartz; they are commonly straight-type necks, but in places they show more complex geometries, i.e. lozenge-shaped, triangular or crescent type (Arslan, Passchier & Koehn, 2008; Fig. 5c) or are represented by tension gashes. Locally the centre of the necking zone hosts an association of syn-kinematic chlorite + sphene + epidote + prismatic oxides +

apatite + minor Na-amphibole + minor albite. Here chlorite is syn- to post- Na-amphibole.

3.b. Brittle structures

3.b.1. Veins

Several sets of veins cut, at a high angle, the mylonitic foliation. We numbered the vein sets from 1 to 5 based on the vein cross-cutting relationships, vein set 1 being the oldest (Fig. 5d). Sets 1 to 3 are syntaxial shear to composite veins and include blueschist-facies assemblages (Fig. 6e, f); sets 4 and 5 are composite veins and developed under later greenschist-facies conditions (see online Supplementary Material, available at <http://journals.cambridge.org/10.1017/S0016756816001163>, and Table S1 therein for a detailed petrographic description).

Vein sets 1 and 2 contain either abundant Na-amphibole + minor epidote and sphene (vein set 1) or Na-amphibole + quartz + white mica + apatite (vein set 2), respectively; both the comparable mineralogical content of boudin necks and vein set 1, and the consistency between the direction of extension indicated by vein set 1 and boudins (Fig. 5d) suggest that the described veining is coeval with boudinage.

We focused in particular on vein set 3, which shows a first opening stage with syn-kinematic Na-amphibole fibres + minor epidote + haematite, followed by albite + epidote + Na-amphibole + white mica + apatite + haematite growth during a second opening stage. We observed that in the wall rock, approaching these veins, albite and Fe-oxide content greatly increases, replacing epidote and Na-amphibole (Fig. 9). Post-kinematic prismatic tiny white mica (paragonite) occurs, partially replaced by albite. This mineralogical variation is reflected by the increase of Na, Mg and Si, and by decreasing Ca and K, moving towards the vein wall. The chemical variation approaching the vein suggests that the wall rock interacted with a fluid that enriched it in Na, Mg and Si and incorporated K and Ca.

3.b.2. Breccia

In some limited horizons and pods, the Na-amphibole-bearing vein network becomes more pervasive and the boudins are progressively disrupted up to brecciation. Such breccia is characterized by clasts of the enclosing MM, with size ranging from <1 cm to a few cm, often sub-rectangular in shape. The breccia is clast-supported, and exhibits angular clasts, with a high clast/matrix ratio; clasts are cemented by inter-clast syn-kinematic Na-amphibole and display a small degree of rotation, attested by the variability in attitude of mylonitic foliation in the different fragments (Fig. 5e, f).

Finally, all the described structures have been deformed and reoriented by later low greenschist-facies

D₃ folds acting at a regional scale (as visible in Fig. 2; Table 1c).

4. Bulk-rock composition

In order to obtain updated *P–T* determinations on the metamorphic conditions, we planned an approach based on the pseudosection method. For the set-up of the method, data on the bulk rock composition and on the mineral chemistry are needed (full details are available in the Supplementary Material).

Bulk-rock composition of both fine-grained (M1M2 sample) and ultra-fine-grained domains (M1M3 sample) has been determined by ICP-MS (inductively coupled plasma mass spectrometry) and INAA (instrumental neutron activation analysis) analyses at Activation Laboratories Ltd (Ontario, Canada) (Table 2; Table S2 in Supplementary Material).

We compared our results with worldwide mid-ocean ridge basalt (MORB) and oceanic gabbro major-element compositions derived from the online PetDB database (<http://www.earthchem.org/petdb>). The analysed samples display variable loss on ignition (LOI) contents, ranging between 1.87 (ultra-fine-grained domains) and 3.51 wt% (fine-grained domains). Major elements have a general MORB affinity, and both samples also fall into the field of oceanic gabbros (Fig. S1, online Supplementary Material at <http://journals.cambridge.org/10.1017/S0016756816001163>). Major-element composition is also comparable to metabasite and meta Fe-gabbro both of the Montenotte and Voltri units (this work; Piccardo, 1977 and references therein; Liou *et al.* 1998; L. Federico, unpub. Ph.D. thesis, Univ. Genova, 2003). Fine- and ultra-fine-grained samples, however, display a lower MgO content, and ultra-fine-grained MM also has a higher Na₂O content.

Rare earth elements (REE), normalized to the chondrite composition (Anders & Ebihara, 1982), are enriched in both samples, with an almost flat pattern and no significant anomalies (Fig. S2 in Supplementary Material). The REE patterns fall into the field of metabasite and eclogite of the Voltri Massif (R. Tribuzio, unpub. Ph.D. thesis, Univ. Pavia, 1992; L. Federico, unpub. Ph.D. thesis, Univ. Genova, 2003), but are mostly comparable to flat patterns of basalts of the northern Apennines (Internal Liguride) which represent the equivalent of the Montenotte and Voltri units metabasite escaped from deep subduction (Rampone, Hofmann & Raczek, 1998).

Figure 10 shows that As and Sb, which are incompatible, fluid-soluble elements, are strongly enriched compared to a MORB composition.

Nb/U vs U and Th/U vs Th diagrams highlight both a U gain and a Th loss compared to fresh MORB (Fig. S3 in Supplementary Material), showing that our samples are in accordance with a seafloor alteration trend as defined for a set of altered oceanic crust rocks and metabasalts (Bebout, 2007 and references therein); our MM thus retained these elements (i.e. U) down to

Table 2. Bulk-rock composition (major elements) of the studied MM and of representative samples of the Montenotte and Voltri units.

	Detection limit	M1M2 MM (wt%)	M1M3B MM (wt%)	260511 Metabasalt (MU) (wt%)	140411 Metagabbro (MU) (wt%)	FP4FP1 Phyllade (MU) (wt%)	070911 Phyllade (MU) (wt%)	TV7TV3 Metagabbro (VU) (wt%)	SP5 Metagabbro (VU) (wt%)	120511 Metabasite (VU) (wt%)	TV6TV3 Metabasite (VU) (wt%)
SiO ₂	0.01	49.42	48.5	50.2	46.06	33.47	47.11	50.67			
Al ₂ O ₃	0.01	15.39	17.07	14.48	10.36	9.88	12.89	14.88			
Fe ₂ O ₃ (T)	0.01	13.32	12.53	10.47	17.99	6.41	14.57	10.3			
MnO	0.001	0.39	0.112	0.144	0.226	0.096	0.298	0.125			
MgO	0.01	4.14	2.36	5.36	5.91	2.68	5.27	6.51			
CaO	0.01	9.11	8.9	9.12	7.01	22.69	9.76	6.9			
Na ₂ O	0.01	2.72	5.3	3.57	4.02	0.5	3.91	3.66			
K ₂ O	0.01	0.22	0.55	0.1	0.08	2.23	< 0.01	0.13			
TiO ₂	0.001	2.242	2.481	2.041	4.899	0.439	5.83	1.674			
P ₂ O ₅	0.01	0.3	0.27	0.24	0.11	0.08	1.01	0.19			
LOI		3.51	1.87	2.69	2.82	20.31	0.39	3.75			
Total		100.8	99.94	98.41	99.48	98.78	101	98.78			

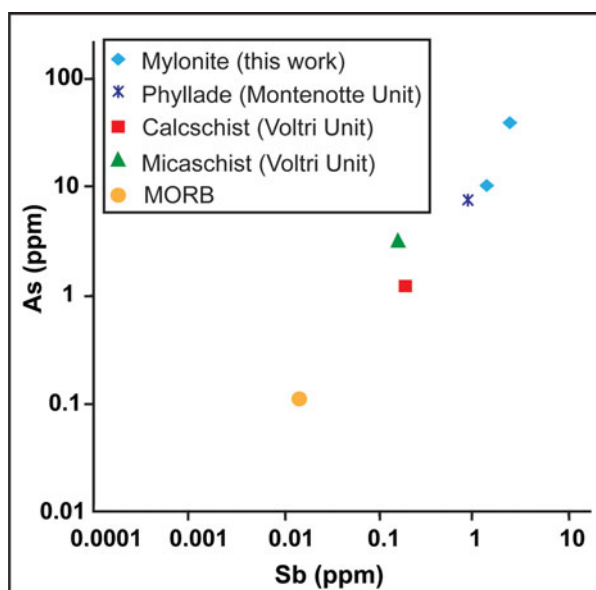


Figure 10. (Colour online) As vs Sb diagram comparing contents of the studied MM with those of metasediments from the Ligurian and Western Alps (explanation in the text). Voltri metasediment data are after Cannò *et al.* (2016); the values of the Montenotte Unit metasediment are unpublished data.

relatively high depths and did not release them into fluids.

5. *P–T* pseudosection

The *P–T* stability conditions of mineral paragenesis along the main mylonitic foliation have been envisaged through *P–T* pseudosections. We selected the bulk-rock composition of sample M1M2 since this was the most homogeneous sample in terms of grain size and the least affected by necks and veins. Pseudosections were calculated using *Perple_X* (Connolly, 1990; www.perplex.ethz.ch) and the internally consistent thermodynamic database of Holland & Powell (1998) as revised by the authors in 2004 (*hp04ver.dat*).

We calculated the stable assemblages in the KCNMTiFMASH system, considering H₂O in excess (*a*H₂O = 1; Fig. 11) and using the equation of state for

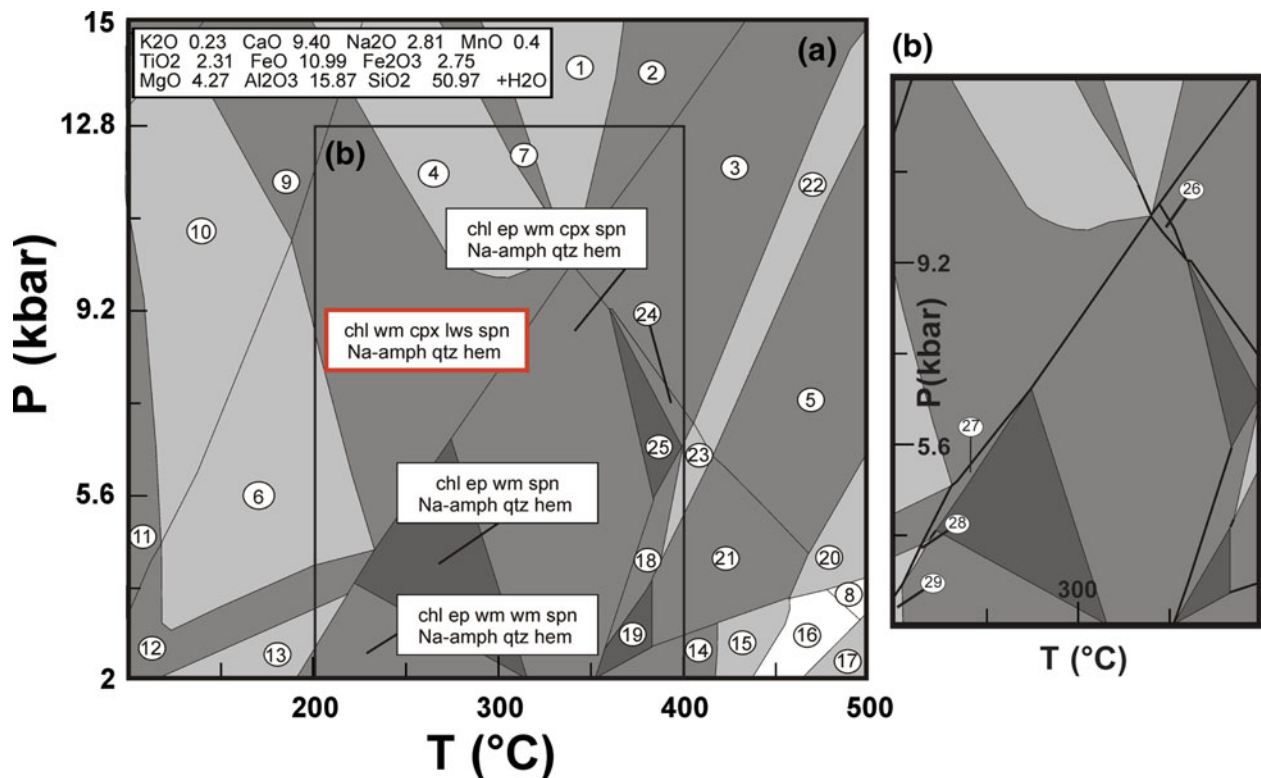
H₂O after Holland & Powell (1998); H₂O is considered in excess because of the occurrence of a high amount of stable hydrated minerals. The used bulk-rock composition matches the effective bulk-rock chemistry as we do not have any mineralogical relics (e.g. magmatic pyroxene or garnet) that could influence the effective bulk rock composition. We neglected CO₂ because the occurrence of sphene instead of rutile implies a very low CO₂ activity (e.g. Castelli *et al.* 2007).

If we consider total iron as FeO, pseudosections do not exactly reproduce the mineralogical associations observed in the sample, especially with reference to epidote stability; we therefore added Fe₂O₃ to the system. In order to estimate the exact Fe³⁺ content in the rock, we produced pseudosections for several fixed Fe₂O₃ amounts (i.e. 10, 20, 40, 50, 60% of Fe_{tot}). The pseudosection that best reproduces the observed mineral assemblage includes Fe₂O₃ = 20% Fe_{tot} (Fig. 11).

We calculated the Na molar fraction in white mica as $X_{Na} = Na/(Na + K)$, and the Fe molar fraction in epidote as $X_{ep} = Fe/(Fe + Al)$. We used the following solid-solution models (*solut_07.dat*): GTrTs and TrTsPg(HP) after White, Powell & Phillips, (2003) and Wei & Powell (2003) for amphibole; Chl(HP) after Holland, Baker & Powell, (1998) for chlorite; Ep(HP) after Holland & Powell (1998) for epidote; Gt(HP) after Holland & Powell (1998) for garnet; Pheng(HP) after Holland & Powell (1998) and KN-Phen after Chatterjee & Froese (1975) for white mica; Cpx(HP) after Zeh *et al.* (2005) and Omph(HP) after Holland & Powell (1996) for clinopyroxene.

The selected pseudosection contains di-, tri-, quadri- and penta-variant fields depicted in light- to dark-grey colours. The assemblage observed in the rock is well described by the field including ep + Na-amph + w-mica + spn + chl + qtz + hem at *c.* *T* = 220–310 °C and *P* = 2–6.5 kbar.

The isopleths of X_{ep} in epidote suggest that the sample crossed a higher *P–T* field (dashed circle in Fig. 12a) characterized by the appearance of a Ca–Na clinopyroxene inside the stability field of Mg-riebeckite. However, because of the presence of



1. chl wm grt cpx lws Na-amph qtz rt hem
2. chl wm grt cpx lws qtz rt hem
3. chl ep wm grt cpx qtz rt hem
4. chl wm cpx lws spn Na-amph qtz rt hem
5. chl ep wm grt cpx qtz rt mag
6. chl wm cpx adr lws spn Na-amph qtz hem
7. chl wm cpx lws Na-amph qtz rt hem
8. chl ep Na-amph wm grt cpx ab qtz rt mag
9. chl wm cpx lws spn Na-amph qtz gt
10. chl wm cpx adr lws spn Na-amph qtz gt
11. chl wm adr lws spn Na-amph qtz gt
12. chl wm adr lws spn Na-amph qtz hem
13. chl wm wm adr lws spn Na-amph qtz hem
14. chl ep wm cpx spn ab qtz mag
15. chl ep wm grt cpx spn ab qtz mag
16. chl ep Na-amph wm grt cpx spn ab qtz mag
17. ep Ca-amph Na-amph wm grt spn ab qtz rt mag
18. chl ep wm cpx spn qtz hem mag
19. chl ep wm cpx spn qtz mag
20. chl ep Na-amph wm grt cpx qtz rt mag
21. chl ep wm grt cpx spn qtz mag
22. chl ep wm grt cpx qtz rt hem mag
23. chl ep wm grt cpx spn qtz hem mag
24. chl ep wm grt cpx spn qtz hem
25. chl ep wm cpx spn qtz hem
26. chl ep wm cpx Na-amph qtz rt hem
27. chl ep wm lws spn Na-amph qtz hem
28. chl ep wm wm lws spn Na-amph qtz hem
29. chl ep wm wm adr spn Na-amph qtz hem

Figure 11. (Colour online) (a) P - T pseudosection using PERPLE_X (sample M1M2). The mineral abbreviations are after Kretz (1983) except for: cpx (clinopyroxene), Na-amph (Na-amphibole), Ca-amph (Ca-amphibole) and wm (white mica). The red box depicts the inferred metamorphic peak conditions. Narrow and small fields have been neglected for the sake of clarity. (b) Detail of the above P - T pseudosection, also including narrow and small fields. Thick lines represent univariant reactions.

lawsonite pseudomorphoses along the foliation, we suggest that the metamorphic peak stage could be represented by the field including Na-amph + w-mica + cpx + lws + spn + chl + qtz + hem; these peak conditions have been restricted using the P - T peak conditions of M1M3 sample, calculated with pseudosection, pointing to $T = 220$ – 310 °C and $P = 6.5$ – 10 kbar (Fig. 13a). The isopleths of Si and X_{Na} content in white mica cross-cut in a low P - T field (solid circle in Figs 12 b,c, 13a) marking the retrogressive stage.

6. Discussion

In the following, we treat (i) the deformative processes that affected the analysed outcrop, (ii) the origin of fluids and fluid-rock interactions, suggesting the pos-

sible correlations among fluids, brittle deformation and seismicity; (iii) finally we propose a geodynamic interpretation for the tectono-metamorphic evolution of the study area.

6.a. Progressive deformation

The occurrence of several superposed structures formed under the same metamorphic conditions suggests that the MM underwent a progressive polyphase deformation history (Fig. 4; Table 1c). The presence of peculiar microstructures such as σ - and δ -type porphyroclasts, and passive folds with a similar geometry (D_1 and D_2 folds; Fig. 4) testifies that deformation in the study area was initially non-coaxial in a shear zone; it evolved in a bulk coaxial deformation (regime of

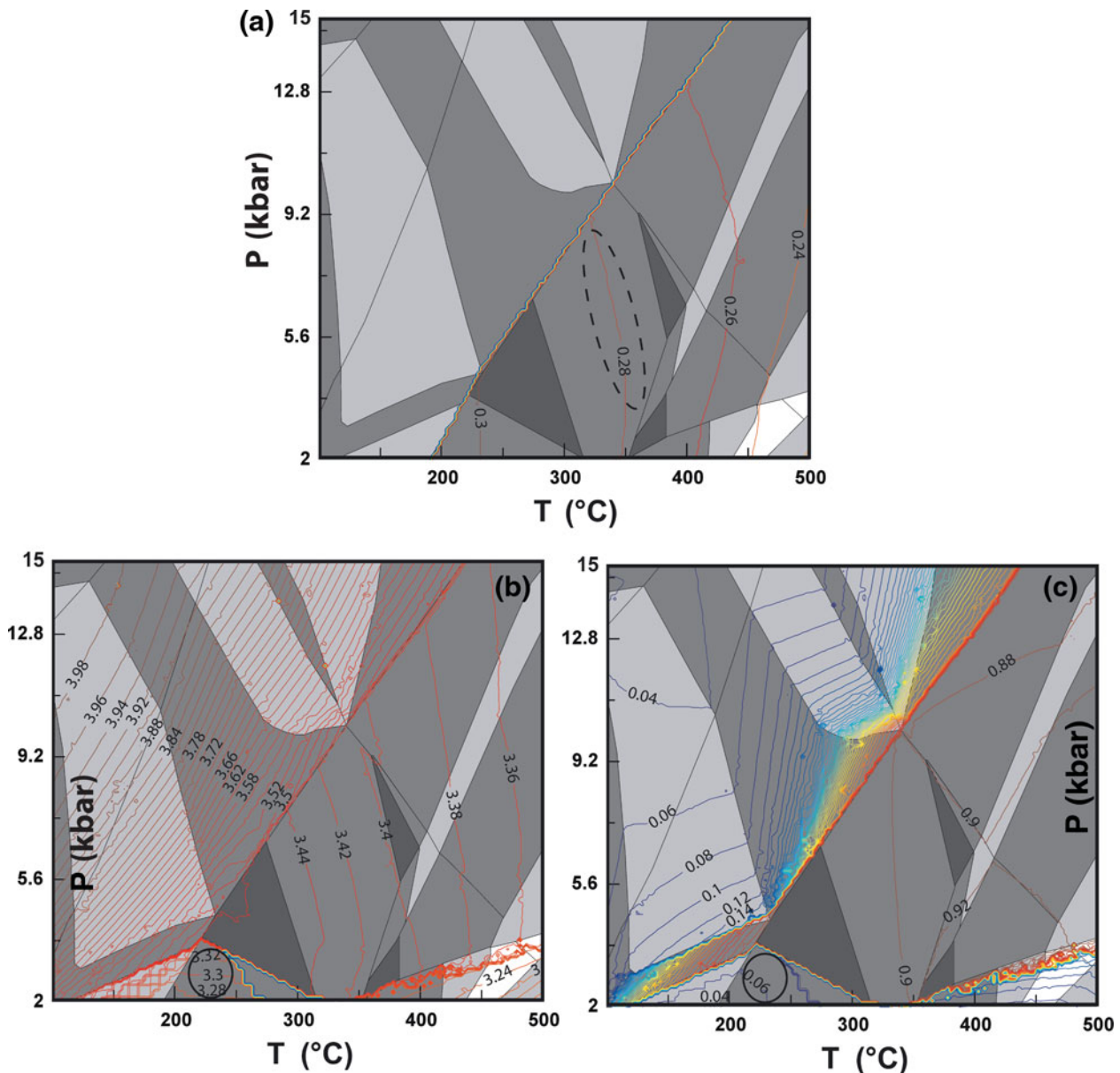


Figure 12. (Colour online) (a) Compositional isopleths for epidote (X_{ep} content); the dashed circle depicts the stability P – T conditions of epidote in our sample. (b, c) Compositional isopleths for white mica (Si and X_{Na} content respectively); the circle shows the stability P – T conditions of white mica in our sample.

general flattening) in the same structural level, producing a “chocolate-table” foliation boudinage. A minor component of shear is suggested by the presence of en échelon tension gashes and shear veins.

The next step in the deformative history is testified by brittle structures, such as veins and breccia. We exclude a primary origin for breccias because clasts contain an internal blueschist mylonitic foliation (Fig. 7b) that does not continue into the breccia cement and must therefore precede the brecciation event.

The transition from ductile deformation (folds; Fig. 5b) to brittle deformation (veining and breccias; Figs 5d, e, 7b) passing through a brittle–ductile regime (foliation boudinage) was therefore gradual; the occurrence of comparable mineral assemblages (Table 1c) along the foliation, in boudin necks, in the first three vein sets and in the breccia cement indicates that such ductile–brittle transition occurred within the same

structural level, without a substantial change in the overall P – T conditions (blueschist-facies metamorphic conditions). The direction of maximum extension derived from the boudins matches one derived by the veins and this corroborates the observation that these deformative events occurred within the same structural setting.

6.b. The role and origin of fluids

6.b.1. The MM–fluids interaction

Figure 10, Table 1 and Figure S4 (Supplementary Material) show that both fine-grained and ultra-fine-grained MM have enriched As, Sb (and Pb) concentrations compared to MORB, and similar or, in the case of As, higher than arc magmas (Hattori & Guillot, 2003). These elements, characterized by a high solubility in

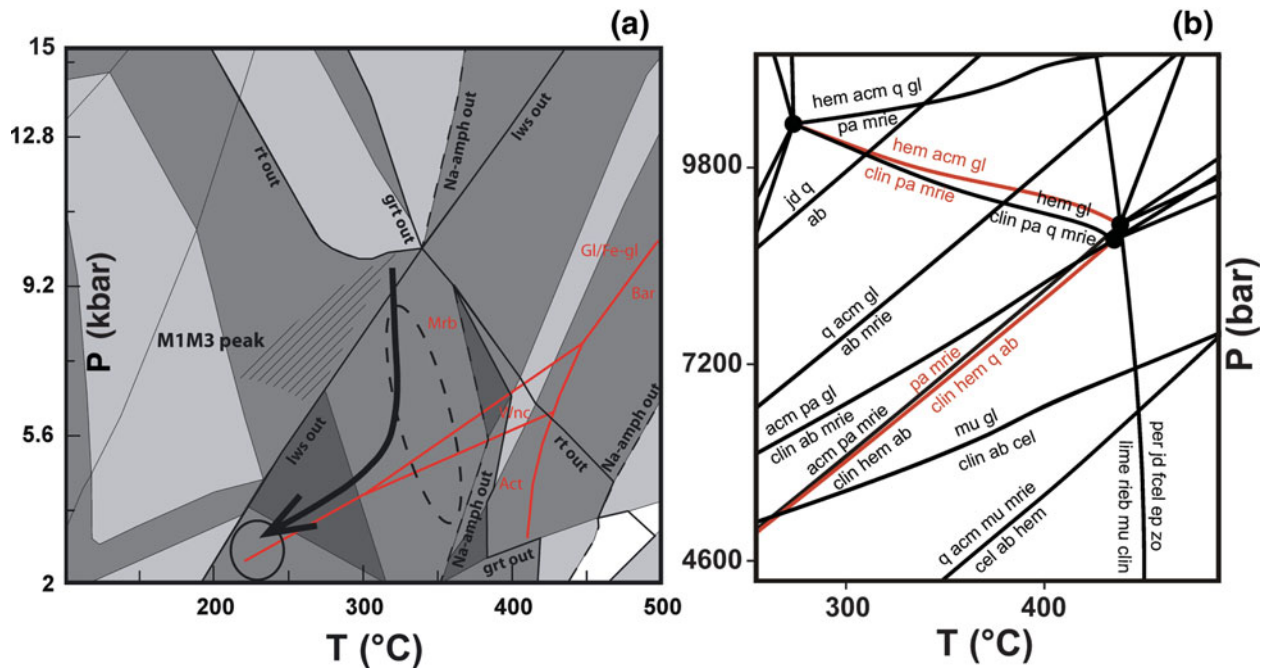


Figure 13. (Colour online) (a) Inferred P - T path for M1M2 sample; the red lines delimit P - T stability fields of amphibole (redrawn after Otsuki & Banno, 1990; Mrb = Mg-riebeckite, Gl/Fe-gl = glaucophane/Fe-glaucophane, Wnc = winckite, Act = actinolite, Bar = barroisite); the solid and dashed circles show the stability P - T conditions of white mica and epidote, respectively. (b) Schreinemaker diagram (KNCFMASH(O) system), drawn using *Perple_X* and the thermodynamic database after Holland & Powell (1998, revised 2004; hp04ver.dat). We considered H_2O in excess ($a_{H_2O} = 1$) and we used the equation of state for H_2O after Holland & Powell (1998). Red lines are the selected reactions.

aqueous fluids at low temperature, can reach high contents in the subducting slab (i.e. metasediments and serpentinite) and are generally released after its dehydration in the forearc mantle wedge during the early stage of subduction and incorporated inside the magmas also enriching volcanic fronts (Hattori & Guillot, 2003; Sadofsky & Bebout, 2003; John *et al.* 2004; Bebout, 2007).

In our rocks, the enrichment in fluid mobile elements, and in particular in As, Sb and Pb, could have several origins. The three main hypotheses are:

- (1) *enrichment of the protolith*: the present composition could simply reflect the composition of the protolith, already enriched in As, Sb and Pb compared to a MORB;
- (2) *ocean-floor alteration*: the present composition could reflect the composition of the protolith that has been enriched by As-Sb-Pb-rich fluids during ocean-floor alteration; our rocks could thus preserve the oceanic fingerprint and have carried fluid mobile elements in subduction at high depths without releasing them;
- (3) *interaction with fluids during subduction*: our rocks could have interacted with external fluids, possibly released by other lithologies during subduction with increasing temperature (i.e. Voltri metasediments; $T_{peak} = 400$ – 500 °C; Cimmino & Messiga, 1979). The fluids were possibly rich in fluid mobile elements (e.g. As and Sb), now stored in amphibole, apatite or Fe-oxide (Smedley & Kinniburgh, 2002).

The first two hypotheses would imply a local-scale fluid circulation restricted to a sort of close chemical system; the third hypothesis would imply an external input of fluids and a large fluid flux.

However, neither the enrichment of the protolith nor the ocean-floor alteration seems to be the case, because both metabasite and metagabbro of the Montenotte Unit, representing the possible undeformed equivalent of the MM, show a very low content of fluid mobile elements (e.g. As, Sb; Fig. 10), suggesting that these elements come from an external source. Moreover P_2O_5 and total iron content in our MM, and in meta-Fe-gabbro, metabasalt of the Montenotte Unit, are comparable, which implies that the high content of fluid mobile elements in the MM is not only related to a higher content of apatite or Fe-oxide. As, Sb and Pb are chalcophile elements, suggesting that sulphides may have some role in their enrichment (Hattori & Guillot, 2003). All our samples, however, contain a very low amount of sulphides (local tiny inclusions in Fe-oxide), and other chalcophile elements such as Cu are not enriched. In addition, Sr and Ce, elements unrelated to sulphides, are also enriched. Therefore, S cannot be considered responsible for the observed enrichment.

Figure 10 shows a distinction between the 'low-grade' metasediments of the Montenotte Unit (phyllade) and those of the Voltri Unit, the latter recording higher metamorphic conditions (Cimmino & Messiga, 1979) and containing a lower amount of As and Sb. Bebout *et al.* (2007) observed that the rocks that experienced high-temperature paths (>350 °C) record a

dramatic depletion of fluid-mobile elements such as Cs, B, As, Sb and N, whereas rocks experiencing the cooler paths largely retain these elements (i.e. lawsonite–albite and lawsonite–blueschist rocks).

The content in As and Sb of our enriched MM falls into the field of low-grade metasediments close to the composition of phyllade, suggesting that the MM may have interacted with external fluids coming from a lithology that suffered dehydration; this lithology may have been the Voltri high-pressure metasediment, which during subduction, with increasing T , progressively discharged fluids rich in incompatible elements, i.e. As and Sb (Hattori & Guillot, 2003). In the literature, serpentinite has been considered as another possible source of hydrous fluid, together with sediments, which infiltrate the slab–mantle interface (Nelson, 1991; Rupke *et al.* 2004; Tenthorey & Hermann, 2004; Ranero *et al.* 2005; Hattori & Guillot, 2007; Spandler *et al.* 2008; Spandler, Pettke & Rubatto, 2011; Angiboust *et al.* 2014). Serpentinite is thought to release hydrous fluids rich in B, As, Sb, Nb, Zr and light rare earth elements (LREE) (Scambelluri *et al.* 2004; Hattori & Guillot, 2007; Spandler, Pettke & Hermann, 2009), and the interaction with serpentinite or serpentinite-derived fluids is responsible for the enrichment in Cr, Ni and Mg (Angiboust *et al.* 2014). Although serpentinite is abundant in the study area and even if we lack in-depth geochemical studies (i.e. B isotopes), in a first approximation we exclude this rock as a possible source of fluids: Cr, Ni and Mg content in the mylonite is in fact comparable to or even lower than (in the case of Mg) ocean-floor gabbro or MORB (Table 1; Fig. S5 in Supplementary Material). Moreover, sediments are generally the first lithology to release fluids even at shallow depths (both pore and crystal lattice water); with increasing temperature, they release fluids more easily with respect to serpentinite that release water at only 650–700 °C at 2–4 GPa (antigorite; Ulmer & Trommsdorff, 1999), which are P – T conditions in any case not reached by our MM; moreover, we did not observe clear signs of dehydration in serpentinite. Furthermore, sediment-derived fluids could also contribute to a second stage of serpentinization during the early stages of subduction at 200–400 °C (Deschamps *et al.* 2011) or could produce significant enrichment of the serpentinite in As, Sb, B and Pb in early subduction stages (Lafay *et al.* 2013; Cannà *et al.* 2015; Scambelluri, Pettke & Cannà, 2015).

6.b.2. Fluids and brittle deformation

As a consequence of ongoing deformation and of primary heterogeneities, the MM is composed of layers of different mineralogies and grain sizes and possibly containing different amounts of free fluids. In particular, the occurrence of ultra-fine-grained layers in the MM may have played a dual role in enhancing fracturing.

- (1) Grain size has been demonstrated to be one of the main factors controlling uniaxial compressive strength in low-porosity rocks (Prikryl, 2001; Villeneuve, Diederichs & Kaiser, 2012): strength increases with decreasing grain size, following a logarithmic law. Moreover, for low-porosity rocks, the stress difference at crack initiation grows with decreasing grain size (Hatzor & Palchik, 1997). Therefore, the ultra-fine-grained domains of the MM may have acted as stress risers (Sibson, 1980), focusing brittle deformation and promoting the formation of breccia horizons.
- (2) Deformation-induced grain-size reduction, which possibly acted in the MM, can also decrease the permeability (Caine, Evans & Foster, 1996) by sealing off the pore spaces (Philipot & Selverstone, 1991). This results in an increase in pore fluid-pressure, which could facilitate the opening of microcracks on a grain scale by reducing the fracture strength of the grain aggregate (Philipot & van Roermund, 1992).

The subsequent cracking, in turn, generates a fluid-pressure drop that causes disequilibrium conditions at the vein walls, and the activation of mineralogical reactions; solution transfer to the vein finally induces mineral precipitation and growth. This is in agreement with the lower LOI content of ultra-fine-grained relative to fine-grained domains. As a consequence, we suggest that differences in grain size and in fluid content between adjacent domains may generate local strain and pore fluid-pressure partitioning; such rheological and fluid-pressure imbalance could have initiated microcrack on a μm to mm scale. Fracturing may therefore be interpreted in terms of brittle instabilities arising from strain and pore-fluid pressure partitioning between adjacent domains of the MM.

In our case, the local fluid-pressure drop triggered reactions that caused the disappearance in the vein wall of Na-amphibole (and phengite), and an increase of the mode of albite and paragonite. Schreinemakers diagrams, produced for the system KNCFMASH using *Perple_X* (Fig. 13b), suggest that paragonite and albite may have formed after the following decompression reactions:

(1) Fe-oxide + Na-pyroxene + Na-amphibole (glaucophane) = chlorite + paragonite + Na-amphibole (Mg-riebeckite)

(2) paragonite + Na-amphibole (Mg-riebeckite) = chlorite + albite + Fe-oxide + quartz

Reaction (1) implies the occurrence of Na-pyroxene, not observed in the present mineralogical assemblage, but occurring in the P – T pseudosection simulated for the composition of our rock (Section 5 above). A Na-pyroxene could have been replaced by Na-amphibole during the development of the present blueschist foliation, with deformation possibly enhancing the disappearance of any textural or mineralogical relics. Na and Mg may not have been completely incorporated in the

solid, and may have remained dissolved in the inter-crystalline fluid, phase, retaining a sort of ‘ghost Napyroxene’ signature; when the fractures formed and the fluid pressure locally dropped, the solution was thus attracted towards the vein, enriching the vein wall in Na and Mg and allowing reaction (1). After the breakdown of phengite and the partial substitution of epidote by albite, the fluid migrating in the vein incorporated K and Ca.

Concerning veins and breccia formation, the fact that the veins and the MM contain identical mineralogy confirms that the scale of fluid and isotopic equilibration was very small, thus arguing for short-range mass-transfer processes (cm-scale fluid-phase diffusional mass transport) and a locally derived fluid rather than fluid infiltration over a relatively large scale, leading to fluid and stable isotope equilibration (Philippot & van Roermund, 1992; Spandler, Pettke & Rubatto, 2011).

Veins thus have a rather contemporaneous growth history, and the scarcity of dehydration reactions in the wall rock suggests that dehydration embrittlement is not a likely mechanism for vein and breccia formation. Confirming this statement, the breccia is characterized by low dilation ratio (the volume ratio between void and clast), angular clasts and only incipient rotation of clasts, thus lacking the typical features of hydraulic breccia (Sibson, 1986; Jébrak, 1997) and suggesting a negligible fluid transport action.

The depth of fracture opening and brecciation can be inferred from the mineral assemblage in the vein infill and breccia matrix; the pressure range of *c.* 2–6.5 kbar, derived by the *P–T* pseudosection fields, suggests that such conditions are in the range 7–20 km (Fig. 13a).

6.b.3. Fluids, fracturing and seismicity

As we have already seen, fracturing may be interpreted in terms of brittle instabilities arising from strain and pore-fluid pressure partitioning. In this way of thinking, the fracture mesh affecting the MM may represent the field evidence of episodic tremors or ‘slow earthquakes’ caused by overpressured fluids at the plate interface (Obara, 2002; Kato 2010; Katayama *et al.* 2012). It has been proposed that high pore pressure provided by hydrous fluids might facilitate faulting by decreasing the friction and thus triggering intermediate-depth seismicity (Davies, 1999 and references therein; Katayama *et al.* 2012).

Sibson (1996) estimated that, to generate a fracture mesh similar to the one described in this paper (disregarding the secondary non-coaxial component) in a compressional setting, we need lithostatic fluid pressure with:

$\lambda_v \approx 1$ (the pore-fluid factor: $\lambda_v = P_f/\sigma_v = P_f/\rho gz$; P_f = fluid pressure, σ_v = vertical stress, ρ = average rock density, g = gravitational acceleration, z = depth) at all depths.

This high pore pressure will reduce the effective normal stresses and promote earthquakes. Several au-

thors have demonstrated that fracture under pressure at low depth results from the coalescence of dilating tensile microcracks (Davies, 1999 and references therein); they propose that isolated pockets of water would nucleate microcracks and water would flow locally to hold them open. With increasing strain, these microcracks would interact to give echelon crack arrays (as we locally observe in our rock), extend and coalesce (Du & Aydin, 1991). This would nucleate rupture, which would then propagate through the water-filled microcracks, leading to substantial slip, stress drop and an earthquake (Davies, 1999). The earthquake, connecting water-filled microcracks, would increase porosity and permeability in the rock (Davies, 1999 and references therein). The set of veins affecting our MM, locally focused in the breccia horizons, could therefore be a record of multiple microcracks occurring during increasing strain and thus possibly originating low-frequency tremors or slow-slip seismic events. This is in agreement with observations and models of slow slip and tremor that require the presence of near-lithostatic pore-fluid pressures in slow-earthquake source regions (Audet & Bürgmann, 2014).

A field setting similar to the one described in this paper, i.e. with relatively strong metabasitic horizons – deforming in a discontinuous manner – enveloped by lower-strength rocks (serpentinites and metasediments) where deformation is accommodated viscously, has been considered a viable source of tremor and slow slip events (Fagereng, Hillary & Diener, 2014; Hayman & Lavier, 2014).

Finally, the occurrence of various vein sets and/or of multiple opening stages in a single set (e.g. set number 3; see Section. 4.2) suggests that these brittle structures likely formed during different successive slow events.

6.b.4. Fluid pressure and geological setting

To achieve veining and brecciation inside the MM, fluids need to have been confined within the mylonitic horizon by the occurrence of a ‘cap rock’ above, possibly serpentinite.

The permeability of the intact MM is difficult to estimate, but is probably very low, in the order of magnitude of that for diabase (De Wiest, 1965), i.e. 10^{-9} darcy (*c.* 10^{-23} m²). However, fractured basaltic rocks have shown *in situ* permeabilities as high as 10^{-2} – 10^2 darcy (*c.* 10^{-16} – 10^{-12} m²; Brace, 1980). In general, it is believed that *in situ* permeability of crystalline rocks is 10^3 greater than laboratory measurements, which represent a measure of the minimum permeability (Brace, 1980). Permeability in serpentinite, in the absence of dehydration due to antigorite breakdown, is estimated at *c.* 10^{-22} m² (Tenthorey & Cox, 2003); in particular, permeability has been shown to vary between 10^{-22} m² perpendicular to foliation and 10^{-20} m² parallel to foliation (Kawano *et al.* 2011). In any case, it is able to act as ‘cap rock’, and therefore

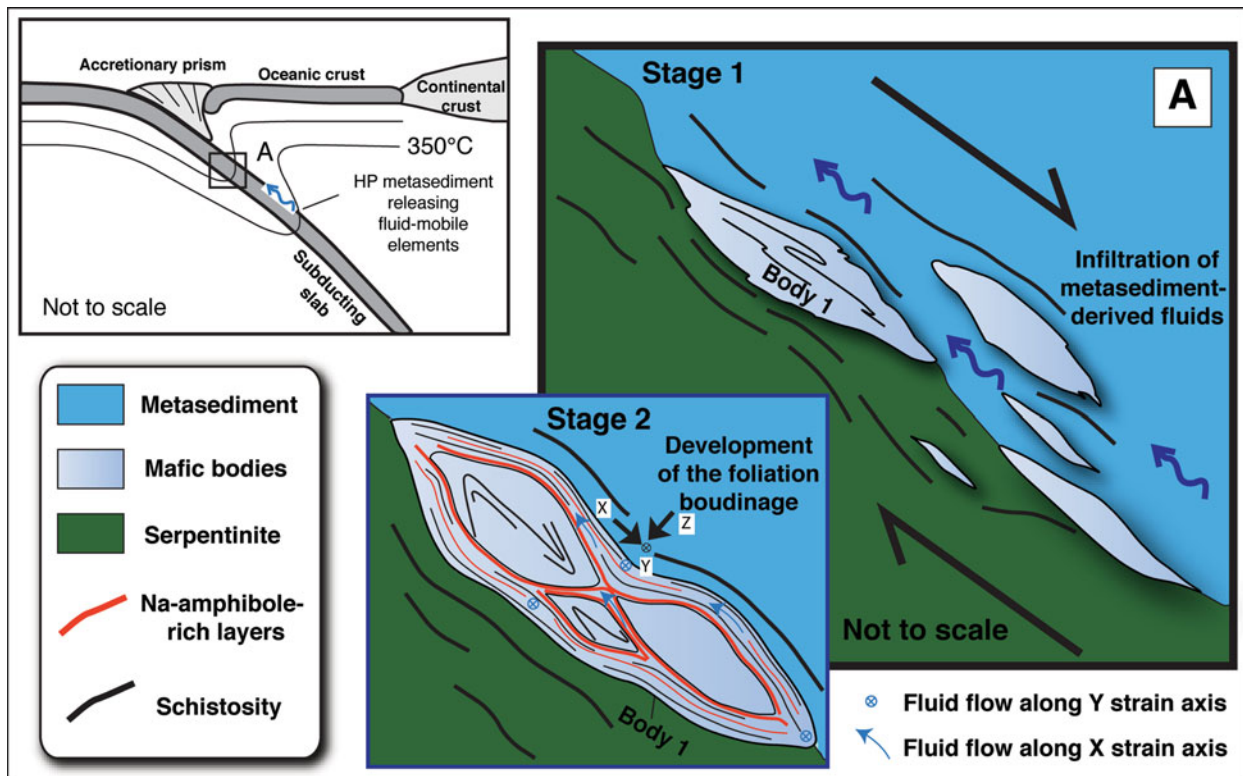


Figure 14. (Colour online) Sketch of the geodynamic evolution of the studied MM. Fluids are shown to flow either along X or Y strain axes. Box A shows a detail of the plate interface.

serpentinite may have acted as a barrier to fluid flow, facilitating the attainment of fluid overpressure inside the MM.

The local dilatancy, associated with fracture opening, will give rise to local pressure gradients between the fractured domains and the immediately surrounding rock (Etheridge *et al.* 1984). These pressure gradients would cause a fluid flow inside the MM, which could potentially be along both X and Y strain axes, in a situation of almost radial extension (Fig. 14).

6.c. Geodynamic implications

The MM horizon that we studied is sandwiched between metasedimentary rocks of the Voltri Unit and serpentinite of the Montenotte Unit, lying respectively at the bottom and at the top of the MM. The observed blueschist mineralogical assemblage (peak conditions at *c.* $T = 220\text{--}310\text{ }^{\circ}\text{C}$ and $P = 6.5\text{--}10\text{ kbar}$) testifies that this rock has been buried during subduction down to crustal depths (*c.* 33 km) (Fig. 13a).

Both chemical and petrographical evidence suggests that during subduction (at least during the development of the former foliation) the MM interacted with external aqueous fluids and behaved like a sponge incorporating them. Fluids were probably released by high-pressure metasediments (i.e. Voltri metasediments) at increasing temperature ($>350\text{ }^{\circ}\text{C}$), during progressive subduction, and percolated upwards along a strongly deforming shear zone probably correspond-

ing to the subducting plate interface or close to it (Fig. 14). This highly deformed mylonitic horizon incorporated the fluids, triggering the development of the hydrous blueschist-facies paragenesis. Previous studies (John *et al.* 2004; Bebout, 2007 and references therein) have shown that intensively deformed zones represent domains of structural weakness, where fluid flux and metasomatism is concentrated, with element gains and losses. Breeding *et al.* (2003) demonstrated that lithologic contacts are important conduits for metamorphic fluid flow in subduction zones. Konrad-Schmolke, O'Brien & Zack, (2011), summarizing a series of natural examples, highlighted that in the slab–mantle transition zone, fluid flux is controlled by the extent of viscous deformation, is channelized in ductile shear zones and is mostly parallel to the slab–mantle interface; here the involved bodies experience a pervasive fluid flow along grain boundaries and a strong fluid–rock interaction.

This evidence suggests that the MM, now outcropping at the border between units in different metamorphic peak conditions, was part of a highly deformed zone, i.e. the plate interface, where an important flux of fluids was active.

7. Concluding remarks

The blueschist-facies MM outcropping between the blueschist-facies Montenotte Unit and the eclogite-facies Voltri Unit (Ligurian Western Alps) is an

example of rock permeated by fluids under high-pressure conditions. This MM probably acted as a shear zone at the contact between units characterized by different metamorphism, probably close to the plate interface in the subduction zone, where chemically reacting fluids preferentially flowed, allowing the enrichment of the MM by incompatible elements (i.e. As, Sb), released by high-grade metasediments. The deformation-induced fracturing, occurring under metamorphic conditions similar to those of the mylonitic foliation development ($T = 220\text{--}310\text{ }^{\circ}\text{C}$ and $P = 2\text{--}6.5\text{ kbar}$), attests that fluids were present at high-pressure blueschist metamorphic conditions. Fracturing here was related to the cycling between ductile deformation, pore-fluid pressure increase and brittle deformation, testifying to a short-range mass-transfer process. Fluids migrated through the body, taking advantage of surfaces along boudins and veins; locally, fracturing was pervasive, producing breccia horizons and a dense mesh of interconnected channels for fluid flow. We finally propose that the fracture mesh affecting the MM is likely a record of past episodic tremors or ‘slow earthquakes’, caused by overpressured fluids.

Acknowledgements. We acknowledge Silvia Torchio for field assistance. This work benefited from the financial support of the PRIN 2010 project ‘Nascita e morte dei bacini oceanici: processi geodinamici dal rifting alla collisione continentale negli Orogeni mediterranei e circum-mediterranei’, national coordinator G. Capponi.

Supplementary material

To view supplementary material for this article, please visit <http://doi.org/10.1017/S0016756816001163>

References

- ABLE, L. & BRADY, J. B. 2001. Lawsonite pseudomorphs in the schists of Syros, Greece. *Geological Society of America, Abstracts with Programs* **33**, A9.
- ANDERS, E. & EBIHARA, M. 1982. Solar system abundances of the elements. *Geochimica et Cosmochimica Acta* **46**, 2363–80.
- ANFOSSI, R., COLELLA, S. & MESSIGA, B. 1984. Posizione strutturale e assetto litologico interno della falda di Montenotte, nella zona compresa tra i torrenti Letimbro e Sansobbia. *Memorie della Societa Geologica Italiana* **28**, 371–84.
- ANGIBOUST, S. & AGARD, P. 2010. Initial water budget: the key to detaching large volumes of eclogitized oceanic crust along the subduction channel? *Lithos* **120**, 453–74.
- ANGIBOUST, S., PETTKE, T., DE HOOG, J. C. M., CARON, B. & ONCKEN, O. 2014. Channelized fluid flow and eclogite-facies metasomatism along the subduction shear zone. *Journal of Petrology* **55**(5), 883–916.
- ARSLAN, A., PASSCHIER, C. W. & KOEHN, D. 2008. Foliation boudinage. *Journal of Structural Geology* **30**, 291–309.
- AUDET, P., BOSTOCK, M. G., BOYARKO, D. C., BRUDZINSKI, M. R. & ALLEN, R. M. 2010. Slab morphology in the Cascadia fore arc and its relation to episodic tremor and slip. *Journal of Geophysical Research* **115**, B00A16. doi: [10.1029/2008JB006053](https://doi.org/10.1029/2008JB006053).
- AUDET, P. & BÜRGMANN, R. 2014. Possible control of subduction zone slow-earthquake periodicity by silica enrichment. *Nature* **510**, 389–92.
- BEBOUT, G. E. 2007. Metamorphic chemical geodynamics of subduction zones. *Earth and Planetary Science Letters* **260**, 373–93.
- BEBOUT, G. E. & BARTON, M. D. 1989. Fluid flow and metasomatism in a subduction zone hydrothermal system: Catalina schist terrane, California. *Geology* **17**, 976–80.
- BEBOUT, G. E. & PENNINGTON-DORLAND, S. C. 2016. Fluid and mass transfer at subduction interfaces – the field metamorphic record. *Lithos* **240–243**, 228–58.
- BECCALUVA, L., MACCIOTTA, G., MESSIGA, B. & PICCARDO, G. B. 1979. Petrology of the Blue-Schists metamorphic ophiolites of the Montenotte Nappe (Western Liguria – Italy). *Ophioliti* **4**, 239–68.
- BOCCHIO, R. 1995. Chemical variations in clinopyroxenes and garnet from eclogites of the Vara Valley (Voltri Group), Italy. *European Journal of Mineralogy* **7**(10), 103–17.
- BRACE, W. F. 1980. Permeability of crystalline and argillaceous rocks. *International Journal of Rock Mechanics and Mining Sciences & Geomechanics Abstracts* **17**(5), 241–51.
- BREEDING, C. M., AGUE, J. J. & BRÖCKER, M. 2004. Fluid–metasedimentary rock interactions in subduction-zone mélange: implications for the chemical composition of arc magmas. *Geology* **32**, 1041–4.
- BREEDING, C. M., AGUE, J. J., BRÖCKER, M. & BOLTON, E. W. 2003. Blueschist preservation in a retrograded, high-pressure, low-temperature metamorphic terrane, Tinos, Greece: implications for fluid flow paths in subduction zones. *Geochemistry, Geophysics, Geosystems* **4**(1), 9002. doi: [10.1029/2002GC0000380](https://doi.org/10.1029/2002GC0000380).
- BROUWER, F. M., VISSERS, R. L. M., & LAMB, W. M. 2002. Metamorphic history of eclogitic metagabbro blocks from a tectonic melange in the Voltri Massif, Ligurian Alps, Italy. *Ophioliti* **27**(1), 1–16.
- CABELLA, R., CORTESOGNO, L., GAGGERO, L. & LUCCHETTI, G. 1994. Clinopyroxenes through the blueschist facies metamorphism of the Liguria Alps: compositional variability and miscibility gaps. *Atti Ticinensi di Scienze della Terra, Serie Speciale* **1**, 55–63.
- CAINE, J. S., EVANS, J. P. & FOSTER, C. B. 1996. Fault zone architecture and permeability structure. *Geology* **24**, 1025–8.
- CANNAÒ, E., AGOSTINI, S., SCAMBELLURI, M., TONARINI, S. & GODARD, M. 2015. B, Sr and Pb isotope geochemistry of high-pressure Alpine metaperidotites monitors fluid-mediated element recycling during serpentinite dehydration in subduction mélange (Cima di Gagnone, Swiss Alps). *Geochimica et Cosmochimica Acta* **163**, 80–100.
- CANNAÒ, E., SCAMBELLURI, M., AGOSTINI, A., TONARINI, S. & GODARD, M. 2016. Linking serpentinite geochemistry with tectonic evolution at the subduction interface: the Voltri Massif case study (Ligurian Western Alps, Italy). *Geochimica et Cosmochimica Acta* **190**, 115–33.
- CAPPONI, G. & CRISPINI, L. 2002. Structural and metamorphic signature of alpine tectonics in the Voltri Massif (Ligurian Alps, northwestern Italy). *Eclogae Geologicae Helveticae* **95**, 31–42.
- CAPPONI, G. & CRISPINI, L. 2008. Note illustrative del Foglio 213–230 ‘Genova’ della Carta Geologica d’Italia alla scala 1:50.000. Apat – Regione Liguria, Italy.

- CAPPONI, G., CRISPINI, L. & FEDERICO, L. (with contributions by CABELLA, R., FACCINI, F., FERRARIS, F., FIRPO, M., ROCCATI, A., MARESCOTTI, P., PIAZZA, M. & SCAMBELLURI, M. and collaboration by DABOVE, G. M., POGGI, E., TORCHIO, S., VIGO, A. & VETUSCHI ZUCCOLINI, M.) 2013. Note illustrative al Foglio 212 'Spigno Monferrato' della Carta Geologica Regionale della Liguria. Retrieved from <http://www.cartografia.regione.liguria.it/>.
- CAPPONI, G., CRISPINI, L., FEDERICO, L. & MALATESTA, C. 2015. Geology of the Eastern Ligurian Alps: a review of the tectonic units. *Italian Journal of Geosciences* **135**(1), 157–69.
- CASTELLI, D., ROLFO, F., GROppo, C. & COMPAGNONI, R. 2007. Impure marbles from the UHP Brossasco-Isasca Unit (Dora-Maira Massif, western Alps): evidence for Alpine equilibration in the diamond stability field and evaluation of the X(CO₂) fluid evolution. *Journal of Metamorphic Geology* **25**, 587–603.
- CHATTERJEE, N. D. & FROESE, E. 1975. A thermodynamic study of the pseudo-binary join muscovite–paragonite in the system KAlSi₃O₈–NaAlSi₃O₈–Al₂O₃–SiO₂–H₂O. *American Mineralogist* **60**, 985–93.
- CHIESA, S., CORTESOGNO, L., FORCELLA, F., GALLI, M., MESSIGA, B., PASQUARÉ, G. & ROSSI, P. M. 1975. Aspetto strutturale ed interpretazione geodinamica del Gruppo di Voltri. *Bollettino della Società Geologica Italiana* **94**(3), 555–82.
- CIMMINO, F. & MESSIGA, B. 1979. I calcescisti del Gruppo di Voltri (Liguria occidentale): le variazioni composizionali delle miche bianche in rapporto alla evoluzione tettono-metamorfica alpina. *Ofoliti* **4**(3), 269–94.
- CONNOLLY, J. 1990. Multivariable phase diagrams: an algorithm based on generalized thermodynamics. *American Journal of Sciences* **290**, 666–718.
- CORTESOGNO, L., GAGGERO, L., LUCCHETTI, G. & CABELLA, R. 2002. Compositional variability and miscibility gap in Na-Ca clinopyroxenes through high pressure metamorphism. *Periodico di Mineralogia* **71**(1), 1–25.
- CRISPINI, L. & FREZZOTTI, M. L. 1998. Fluid inclusion evidence for progressive folding during decompression in metasediments of the Voltri Group (Western Alps, Italy). *Journal of Structural Geology* **20**(12), 1733–46.
- DAVIES, J. H., 1999. The role of hydraulic fractures and intermediate-depth earthquakes in generating subduction-zone magmatism. *Nature* **398**, 142–5.
- DESCHAMPS, F., GUILLOT, S., GODARD, M., ANDREANI, M. & HATTORI, K. 2011. Serpentinites act as sponges for fluid-mobile elements in abyssal and subduction zone environments. *Terra Nova* **23**, 171–8.
- DESMONS, J., COMPAGNONI, R. & CORTESOGNO, L. 1999. Alpine metamorphism of the Western Alps: II. High P/T and related pre-greenschist metamorphism. *Schweizerische Mineralogische und Petrografische Mitteilungen* **79**, 111–34.
- DE WIEST, R. J. M. 1965. *Geohydrology*. New York: John Wiley, 366 pp.
- DU, Y. & AYDIN, A., 1991. Interaction of multiple cracks and formation of echelon crack arrays. *International Journal for Numerical and Analytical Methods in Geomechanics* **15**(3), 205–18.
- ERNST, W. G. 1976. Mineral chemistry of eclogites and related rocks from the Voltri Group, Western Liguria, Italy. *Schweizerische Mineralogische und Petrografische Mitteilungen* **56**, 293–343.
- ETHERIDGE, M. A., WALL, V. J., COX, S. F. & VERNON, R. H., 1984. High fluid pressures during regional metamorphism and deformation: implications for mass transport and deformation mechanisms. *Journal of Geophysical Research* **89**(B6), 4344–58.
- FAGERENG, Å., HILLARY, G. W. B. & DIENER, J. F. A. 2014. Brittle-viscous deformation, slow slip, and tremor. *Geophysical Research Letters* **41**, 4159–67.
- FARYAD, S. W. & HOINKES, G. 1999. Two contrasting mineral assemblages in the Meliata blueschists, Western Carpathians, Slovakia. *Mineralogical Magazine* **63**(4), 489–501.
- FEDERICO, L., CAPPONI, G., CRISPINI, L. & SCAMBELLURI, M. 2004. Exhumation of alpine high pressure rocks: insights from petrology of eclogite clasts in the Tertiary Piedmontese basin (Ligurian Alps, Italy). *Lithos* **74**(1–2), 21–40.
- FEDERICO, L., CAPPONI, G., CRISPINI, L., SCAMBELLURI, M. & VILLA, I. M. 2005. ³⁹Ar/⁴⁰Ar dating of high-pressure rocks from the Ligurian Alps: evidence for a continuous subduction–exhumation cycle. *Earth and Planetary Science Letters* **240**, 668–80.
- FEDERICO, L., CRISPINI, L., MALATESTA, C., TORCHIO, S. & CAPPONI, G. 2014. Geology of the Pontinvrea area (Ligurian Alps, Italy): structural setting of the contact between Montenotte and Voltri units. *Journal of Maps* **11**(1), 1–13. doi: [10.1080/17445647.2014.945749](https://doi.org/10.1080/17445647.2014.945749).
- FEDERICO, L., CRISPINI, L., SCAMBELLURI, M. & CAPPONI, G., 2007. Ophiolite mélange zone records exhumation in a fossil subduction channel. *Geology* **35**(6), 499–502.
- FORD, M., DUCHÊNE, S. & GASQUET, D. 2006. Two-phase orogenic convergence in the external and internal SW Alps. *Journal of the Geological Society* **163**, 815–26.
- GAO, J. & KLEMD, R. 2001. Primary fluids entrapped at blueschist to eclogite transition; evidence from the Tianshan meta-subduction complex in northwestern China. *Contributions to Mineralogy and Petrology* **142**(1), 1–14.
- GHOSH, S. K. & SENGUPTA, S. 1987. Progressive development of structures in a ductile shear zone. *Journal of Structural Geology* **9**(3), 277–87.
- HACKER, B. R., PEACOCK, S. M., ABERS, G. A. & HOLLOWAY, S. D. 2003. Subduction factory 2. Are intermediate-depth earthquakes in subducting slabs linked to metamorphic dehydration reactions? *Journal of Geophysical Research* **108**, 1–16.
- HATTORI, K. H. & GUILLOT, S. 2003. Volcanic fronts form as a consequence of serpentinite dehydration in the forearc mantle wedge. *Geology* **31**(6), 525–8.
- HATTORI, K. & GUILLOT, S. 2007. Geochemical character of serpentinites associated with high- to ultrahigh-pressure rocks in the Alps, Cuba, and the Himalayas: recycling of elements in subduction zones. *Geochemistry, Geophysics, Geosystems* **8**, Q09010. doi: [10.1029/2007GC001594](https://doi.org/10.1029/2007GC001594).
- HATZOR, Y. H. & PALCHIK, V. 1997. The influence of grain size and porosity on crack initiation stress and critical flaw length in dolomites. *International Journal of Rock Mechanics and Mining Sciences* **34**(5), 805–16.
- HAYMAN, N. W. & LAVIER, L. L. 2014. The geologic record of deep episodic tremor and slip. *Geology* **42**(3), 195–8.
- HOLLAND, T., BAKER, J. & POWELL, R. 1998. Mixing properties and activity–composition relationships of chlorites in the system MgO–FeO–Al₂O₃–SiO₂–H₂O. *European Journal of Mineralogy* **10**, 395–406.
- HOLLAND, T. & POWELL, R. 1996. Thermodynamics of order–disorder in minerals. Symmetric formalism applied to solid solutions. *American Mineralogist* **81**, 1425–37.

- HOLLAND, T. & POWELL, R. 1998. An internally consistent thermodynamic data set for phases of petrological interest. *Journal of Metamorphic Geology* **16**, 309–43.
- JÉBRAK, M. 1997. Hydrothermal breccias in vein-type ore deposits: a review of mechanisms, morphology and size distribution. *Ore Geology Reviews* **12**(3), 111–34.
- JOHN, T., KLEMD, R., GAOD, J. & GARBE-SCHÖNBERG, C. D. 2008. Trace-element mobilization in slabs due to non steady-state fluid–rock interaction: constraints from an eclogite-facies transport vein in blueschist (Tianshan, China). *Lithos* **103**, 1–24.
- JOHN, T., SCHERER, E., HAASE, K. M. & SCHENK, V. 2004. Trace element fractionation during fluid-induced eclogitization in a subducting slab: trace element and Lu–Hf/Sm–Nd isotope systematics. *Earth and Planetary Science Letters* **227**, 441–56.
- KATAYAMA, I., TERADA, T., OKAZAKI, K. & TANIKAWA, W. 2012. Episodic tremor and slow slip potentially linked to permeability contrasts at the Moho. *Nature Geoscience* **5**(10), 731–4. doi: [10.1038/NNGEO1559](https://doi.org/10.1038/NNGEO1559).
- KATO, A. 2010. Variation of fluid pressure within the subducting oceanic crust and slow earthquakes. *Geophysical Research Letters* **37**, L14310. doi: [10.1029/2010GL043723](https://doi.org/10.1029/2010GL043723).
- KAWANO, S., KATAYAMA, I. & OKAZAKI, K. 2011. Permeability anisotropy of serpentinite and fluid pathways in a subduction zone. *Geology* **39**, 939–42.
- KONRAD-SCHMOLKE, M., O'BRIEN, P. J. & ZACK, T. 2011. Fluid migration above a subducted slab: constraints on amount, pathways and major element mobility from partially overprinted eclogite-facies rocks (Sesia Zone, Western Alps). *Journal of Petrology* **52**(3), 457–86.
- KRETZ, R. 1983. Symbols for rock-forming minerals. *American Mineralogist* **68**, 277–9.
- LAFAY, R., DESCHAMPS, F., SCHWARTZ, S., GUILLOT, S., GODARD, M., DEBRET, B. & NICOLLET, C. 2013. High-pressure serpentinites, a trap-and-release system controlled by metamorphic conditions: example from the Piedmont zone of the Western Alps. *Chemical Geology* **343**, 38–54.
- LEAKE, B. E., WOOLLEY, A. R., ARPS, C. E. S., BIRCH, W. D., GILBERT, M. C., GRICE, J. D., HAWTHORNE, F. C., KATO, A., KISCH, H. J., KRIVOVICHEV, V. G., LINTHOUT, K., LAIRD, J., MANDARINO, J. A., MARESCH, W. V., NICKEL, E. H., ROCK, N. M. S., SCHUMACHER, J. C., SMITH, D. C., STEPHENSON, N. C. N., UNGARETTI, L., WHITTAKER, E. J. W. & YOUZHI, G., 1997. Nomenclature of amphiboles: report of the subcommittee on amphiboles of the international mineralogical association, commission on new minerals and mineral names. *The Canadian Mineralogist* **35**, 219–46.
- LE PICHON, X., HENRY, P. & LALLEMANT, S. 1990. Water flow in the Barbados accretionary complex. *Journal of Geophysical Research: Solid Earth* **95**, 8945–67.
- LI, Y., MASSONNE, H. J., WILLNER, A., TANG, H. F. & LIU, C. Q. 2008. Dehydration of clastic sediments in subduction zones: theoretical study using thermodynamic data of minerals. *Island Arc* **17**, 577–90.
- LIU, J. G., ZHANG, R., ERNST, W. G., LIU, J. & MCLIMANS, R. 1998. Mineral parageneses in the Piampaludo eclogitic body, Gruppo di Voltri, Western Ligurian Alps. *Schweiz. Mineralogische und Petrographische Mitteilungen* **78**, 317–35.
- MALATESTA, C., CRISPINI, L., FEDERICO, L., CAPPONI, G. & SCAMBELLURI, M. 2012a. The exhumation of high pressure ophiolites (Voltri Massif, Western Alps): insights from structural and petrologic data on meta-gabbro bodies. *Tectonophysics* **568/569**, 102–23.
- MALATESTA, C., GERYA, T., SCAMBELLURI, M., CRISPINI, L. & CAPPONI, G., 2012b. Intraoceanic subduction of 'heterogeneous' oceanic lithosphere in narrow basins: 2D numerical modeling. *Lithos* **140–141**, 234–51.
- MESSIGA, B., PICCARDO, G. B. & ERNST, W. G. 1983. High pressure Eo-Alpine parageneses developed in magnesian metagabbros, Gruppo di Voltri, Western Liguria, Italy. *Contributions to Mineralogy and Petrology* **83**, 1–15.
- MOORE, J. C. & VROLIJK, P. 1992. Fluids in accretionary prisms. *Reviews of Geophysics* **30**, 113–35.
- NELSON, B. K. 1991. Sediment-derived fluids in subduction zones: isotopic evidence from veins in blueschist and eclogite of the Franciscan Complex, California. *Geology* **19**(10), 1033–6.
- OBARA, K. 2002. Nonvolcanic deep tremor associated with subduction in southwest Japan. *Science* **296**(5573), 1679–81.
- OTSUKI, M. & BANNO, S. 1990. Prograde and retrograde metamorphism of hematite-bearing basic schists in the Sanbagawa belt in central Shikoku. *Journal of Metamorphic Geology* **8**, 425–39.
- PEACOCK, S. M. 1993. The importance of blueschist to eclogite dehydration reactions in subducting oceanic crust. *Geological Society of America Bulletin* **105**, 684–94.
- PHILIPPOT, P. & SELVERSTONE, J. 1991. Trace-element-rich brines in eclogitic veins: implications for fluid composition and transport during subduction. *Contributions to Mineralogy and Petrology* **106**, 417–30.
- PHILIPPOT, P. & VAN ROERMUND, H. L. M. 1992. Deformation processes in eclogitic rocks: evidence for the rheological delamination of the oceanic crust in deeper levels of subduction zones. *Journal of Structural Geology* **14**(8–9), 1059–77.
- PICCARDO, G. 1977. Le ofioliti dell'areale ligure: petrologia e ambiente geodinamico di formazione. *Rendiconti Società Italiana di Mineralogia e Petrologia* **33**(1), 221–52.
- POLINO, R., DAL PIAZ, G. V. & GOSSO, G. 1990. Tectonic erosion at the Adria margin and accretionary processes for the Cretaceous orogeny of the Alps. Paris/Zürich/Rome: Société Géologique de France/Société Géologique Suisse/Società Geologica Italiana, pp. 345–67. Memoir no. 156 (new series)/no. 1/special volume.
- PRIKRYL, R. 2001. Some microstructural aspects of strength variation in rocks. *International Journal of Rock Mechanics & Mining Sciences* **38**, 671–82.
- RAMPONE, E., HOFMANN, A. W. & RACZEK, I. 1998. Isotopic contrasts within the Internal Liguride ophiolite (N. Italy): the lack of a genetic mantle–crust link. *Earth and Planetary Science Letters* **163**, 175–89.
- RAMPONE, E., ROMAIRONE, A., ABOUCHAMI, W., PICCARDO, G. B. & HOFMANN, A. W. 2005. Chronology, petrology and isotope geochemistry of the Erro–Tobbio peridotites (Ligurian Alps, Italy): records of Late Palaeozoic lithospheric extension. *Journal of Petrology* **46**(4), 799–827.
- RAMSAY, J. G. & HUBER, M. I. 1987. *The Techniques of Modern Structural Geology, vol. 2: Folds and Fractures*. London: Academic Press.
- RANERO, C. R., VILLASENOR, A., PHIPPS MORGAN, J. & WEINREBE, W. 2005. Relationship between bend-faulting at trenches and intermediate-depth seismicity.

- Geochemistry, Geophysics, Geosystems* **6**, Q12002. doi: [10.1029/2005GC000997](https://doi.org/10.1029/2005GC000997).
- RUBATTO, D. & HERMANN, J. 2003. Zircon formation during fluid circulation in eclogites (Monviso, Western Alps): implications for Zr and Hf budget in subduction zones. *Geochimica et Cosmochimica Acta* **67**, 2173–87.
- RUPKE, L. H., MORGAN, J. P., HORT, M. & CONNOLLY, J. A. D. 2004. Serpentine and the subduction zone water cycle. *Earth and Planetary Science Letters* **223**, 17–34.
- SADOFSKY, S. J. & BEBOUT, G. E. 2003. Record of fore-arc devolatilization in low-T, high-P/T metasedimentary suites: significance for models of convergent margin chemical cycling. *Geochemistry, Geophysics, Geosystems* **4**(4), 9003. doi: [10.1029/2002GC000412](https://doi.org/10.1029/2002GC000412).
- SCAMBELLURI, M., BEBOUT, G. E., BELMONTE, D., GILIO, M., CAMPOMENOSI, N., COLLINS, N. & CRISPINI, L. 2016. Carbonation of subduction-zone serpentinite (high-pressure ophiocarbonate; Ligurian Western Alps) and implications for the deep carbon cycling. *Earth and Planetary Science Letters* **441**, 155–66.
- SCAMBELLURI, M., FIEBIG, J., MALASPINA, N., MÜNTENER, O. & PETTKE, T. 2004. Serpentine subduction: implications for fluid processes and trace element recycling. *International Geology Review* **46**, 595–613.
- SCAMBELLURI, M., PETTKE, T. & CANNAÒ, E. 2015. Fluid-related inclusions in Alpine high-pressure peridotite reveal trace element recycling during subduction-zone dehydration of serpentinitized mantle (Cima di Gagnone, Swiss Alps). *Earth and Planetary Science Letters* **429**, 45–59.
- SCAMBELLURI, M., PETTKE, T., RAMPONE, E., GODARD, M. & REUSSER, E. 2014. Petrology and trace element budgets of high-pressure peridotites indicate subduction dehydration of serpentinitized mantle (Cima di Gagnone, Central Alps, Switzerland). *Journal of Petrology* **55**, 459–98.
- SCAMBELLURI, M., STRATING, E. H. H., PICCARDO, G., VISSERS, R. L. M. & RAMPONE, E. 1991. Alpine olivine- and titanite clinohumite-bearing assemblages in the Erro-Tobbio peridotite (Voltri Massif, NW Italy). *Journal of Metamorphic Geology* **9**, 79–91.
- SCAMBELLURI, M. & TONARINI, S. 2012. Boron isotope evidence for shallow fluid transfer across subduction zones by serpentinitized mantle. *Geology* **40**(10), 907–10.
- SCHMIDT, M. W. & POLI, S. 1998. Experimentally based water budgets for dehydrating slabs and consequences for arc magma generation. *Earth and Planetary Science Letters* **163**, 361–79.
- SIBSON, R. H. 1980. Transient discontinuities in ductile shear zones. *Journal of Structural Geology* **2**, 1–2, 165–71.
- SIBSON, R. H. 1986. Brecciation processes in fault zones: inferences from earthquake rupturing. *Pageoph* **124**, 1–2.
- SIBSON, R. H. 1996. Structural permeability of fluid-driven fault-fracture meshes. *Journal of Structural Geology* **18**(8), 1031–42.
- SMEDLEY, P. L. & KINNIBURGH, D. G. 2002. A review of the source, behaviour and distribution of arsenic in natural waters. *Applied Geochemistry* **17**(5), 517–68.
- SPANDLER, C., HERMANN, J., FAURE, K., MAVROGENES, J. & ARCULUS, R. 2008. The importance of talc and chlorite-hybrid rocks for volatile recycling through subduction zones; evidence from the high-pressure subduction mélange of New Caledonia. *Contributions to Mineralogy and Petrology* **155**, 181–98.
- SPANDLER, C., PETTKE, T. & HERMANN, J. 2009. The composition of serpentinite dehydration fluids in subduction zones: an experimental study. *Geochimica et Cosmochimica Acta* **73**, Supplement 1, A1256.
- SPANDLER, C., PETTKE, T. & RUBATTO, D. 2011. Internal and external fluid sources for eclogite-facies veins in the Monviso meta-ophiolite, Western Alps: implications for fluid flow in subduction zones. *Journal of Petrology* **52**(6), 1207–36.
- TENTHOREY, E. & COX, S. F., 2003. Reaction-enhanced permeability during serpentinite dehydration. *Geology* **31**(10), 921–4.
- TENTHOREY, E. & HERMANN, J. 2004. Composition of fluids during serpentinite breakdown in subduction zones: evidence for limited boron mobility. *Geology* **32**, 865–8.
- ULMER, P. & TROMMSDORFF, V. 1999. Phase relations of hydrous mantle subducting to 300 km. In *Mantle Petrology: Field Observations and High-Pressure Experimentation* (eds Y. Fei, C. M. Bertka & B. Mysen), pp. 259–81. Special Publications of the Geochemical Society no. 6.
- VANOSI, M., CORTESOGNO, L., GALBIATI, B., MESSIGA, B., PICCARDO, G. & VANNUCCI, R. 1984. Geologia delle Alpi Liguri: dati, problemi, ipotesi. *Memorie della Società Geologica Italiana* **28**, 5–75.
- VILLENEUVE, M., DIEDERICHS, M. & KAISER, P. 2012. Effects of grain scale heterogeneity on rock strength and the chipping process. *International Journal of Geomechanics* **12**, Special issue: Advances in Modeling Rock Engineering Problems, 632–47.
- WEI, C. J. & POWELL, R. 2003. Phase relations in high-pressure metapelites in the system KFMASH (K₂O–FeO–MgO–Al₂O₃–SiO₂–H₂O) with application to natural rocks. *Contributions to Mineralogy and Petrology* **145**, 301–15.
- WHITE, R. W., POWELL, R. & PHILLIPS, G. N. 2003. A mineral equilibria study of the hydrothermal alteration in mafic greenschist facies rocks at Kalgoorlie, Western Australia. *Journal of Metamorphic Geology* **21**, 455–68.
- ZEH, A., HOLLAND, T. J. B. & KLEMD, R. 2005. Phase relationships in grunerite–garnet-bearing amphibolites in the system CFMASH, with applications to metamorphic rocks from the Central Zone of the Limpopo Belt, South Africa. *Journal of Metamorphic Geology* **23**(1), 1–17.